Table of Contents

		Page	
I	Summary	1	1/A7
II	Introduction	2	1/A8
III	Separator Study Machine	3	1/A9
IV	Test Bearings	6	1/A12
V	Separator Force Transducer	6	1/A12
VI	Force Transducer Calibration	7	1/A13
VII	Experimental Procedure	7	1/A13
VIII	Data Analysis	8	1/A14
IX	Results and Discussion	11	1/B3
	A. Roller to Cage Contact Forces	12	1/B4
	B. Cage to Inner Race Land Contact Force	14	1/B6
	C. Cage to Shaft Speed Ratios	15	1/B7
X	Summary of Results	15	1/B7
XI	References	16	1/B8

Letter 830-H-14

NASA 1.26:3048

SEP 26 1978

NASA Contractor Report 3048

COMPLETED
ORIGINAL

Microfilmed From
Best Available Copy

Roller to Separator Contact Forces and Cage to Shaft Speed Ratios in Roller Bearings

Lester J. Nypan

GRANT NSG-3065
SEPTEMBER 1978

NASA

Glenn 838-H-14 NAS 1.26:3048

NASA Contractor Report 3048

Microfilmed From
Best Available Copy

Roller to Separator Contact Forces and Cage to Shaft Speed Ratios in Roller Bearings

Lester J. Nypan
California State University, Northbridge
Northbridge, California

Prepared for
Lewis Research Center
under Grant NSG-3065

National Aeronautics
and Space Administration

Scientific and Technical
Information Office

1978

Blank Page

List of Figures

Figure		Page
1a	Separator Study Machine	17
1b	Schematic of Shaft Assembly	18
1c	Light Path Through The Scanner	19
2	Sample Force Transducer Calibration	20
3	Roller Contact Forces 0.18 mm Clearance Bearing	21
4	Roller Contact Forces 0.21 mm Clearance Bearing	41
5	Roller Contact Forces Out-of-Round Outer Raceway Bearing	50
6	Resultant Cage Force Location Versus Shaft Speed	61
7	Cage to Shaft Speed Ratios	63

List of Tables

Table		Page
1	Test Bearing Specifications	65
2	Summary of Test Conditions and Data	66
3	Calculated Number of Shaft Revolutions Between Photographs For Bearing with Epicyclic Speed Ratio of 0.456	67

I Summary

Cage to roller force measurements, cage to shaft forces, and cage to shaft speed ratios are reported for 115 and 118mm bore roller bearings operating at speeds of 4,000, 8,000, and 12,000 rpm under loads ranging from 360 to 6670 N (80 to 1500 lb).

II Introduction

Current developments in jet engine technology are placing more stringent demands on gas turbine design. There is a constantly increasing requirement for engines to develop greater thrust outputs. In addition to this increased loading the need to raise the thrust/weight ratio of engines and to improve the fuel consumption has led to higher rotor speeds and operating temperatures, lighter components and correspondingly increased structural flexibility. In anticipation of tomorrow's requirements, further advanced knowledge of engine component technology must be obtained.(1)*

In the case of rolling contact bearings there is a need for a better understanding of cage and rolling element dynamics, particularly in ultra-high speed applications.(2,3,4,5)

Recently developed, advanced bearing theories have resulted in computerized optimization of rolling element bearing designs and in some cases accurate prediction of bearing performance. These developments and advances by no means substitute for testing of rolling element bearings which for many years was the basis for bearing development. To the contrary, the need for more refined data gathering methods has become obvious. Tests are needed to verify the theories which form the foundation of these computer programs. Also, performance tests and studies will always be needed to refine bearing designs for critical applications.

The interaction between the rolling elements of a bearing with the raceways and separators is particularly difficult to measure due

---

*Numbers in parentheses designate references at end of report.

to the rapidity of their motion. The kinematic behavior and the resulting forces acting on a rolling element/separator/raceway assembly could in the past be measured only by tests where the operating conditions were drastically simplified.

III Separator Study Machine

An optical bearing test rig has been constructed to operate the bearing and make photographic records of the rolling elements and separator behavior. Figure 1a shows an overall view of the machine as it is presently installed in the Dynamics Laboratory of the Engineering Building at California State University, Northridge. The machine was originally assembled by Industrial Tectonics, Inc., Compton, Calif., and has been used in industrial bearing research, and in a ball motion study reported in (6), and in a ball to cage force study (7).

The bearing test rig is basically a shaft supported by a pair of preloaded ball bearings at one end and the test bearing at the other end. One face of the test bearing is exposed to allow free view of the rollers and the separator. Radial load is applied to the test bearing by a hydraulic actuator through a cable loop over the bearing housing. The shaft is driven by a 75 hp hydraulic motor through a geared belt drive, giving speeds infinitely variable from 100 to 15,000 rpm. Figure 1b is a schematic of the shaft assembly.

Lubricating oil for under race cooling and test bearing lubrication is supplied through a series of orifices from the rear of the test bearing.

Due to the high tangential velocities present when a bearing is rotated at shaft speeds up to 12,000 rpm, conventional photograph techniques are inadequate. The difficulty lies in obtaining photo-

graphs having sufficient resolution for analysis when very short exposures are required to freeze the motion of the bearing elements. This problem has been overcome by eliminating the gross rotational motion using a derotation prism. The resulting image thus presents the differential motion between the separator and the rolling element, enabling observation and photographs to be made of an individual separator pocket. Derotation is accomplished by synchronizing the rotation of a Pechan prism at half-speed with the rotation of the roller separator, thus causing the apparent image rotation and the true separator rotation to coincide. This results in the derotated image of the area of interest being imaged on the film plane of a camera. Light rays from the illuminated bearing are collected through the front window of the instrument. This window is optically coated to reject ultraviolet energy produced by ultraviolet lamps, serving the circuit for the prism speed control. From the window, the rays travel through collimator lenses and the Pechan prism before they travel through the exit lenses. Their path is then deflected by mirrors which fold the image in different directions. Figure 1c shows light paths through the scanner.

One light trace travels to a beam splitter where approximately 15 % of the light is reflected to the eyepiece optics to provide an image observable to the operator. The balance of light enters the aperture of the pulse camera.

Alignment and positioning of the optical elements ensure that the eyepiece observes the same image quality and format as that which the film sees.

Another image is folded and demagnified in the transfer lens assembly before it enters a high speed camera when one is used.

A derotated image of the luminous painted segment of the test bearing separator is optically folded out and directed toward an

image splitting mirror surface wedge which proportions the light entering two photomultiplier tube photocathodes. The electronic signals from these tubes are used by the tracking system to control the prism speed.

A tracking system holds the image of a selected point at the test bearing separator in the field of view. It will accommodate a variation of up to 10% of a fixed ratio of separator-to-shaft speed without loss of the ability to lock onto the proper position within one revolution of the bearing retainer.

It is necessary to sense the tracking error in angular position of the derotation prism to provide an input for the servo system. This error signal is provided in the form of the difference in output of the two multiplier phototubes.

A sector on the bearing retainer is coated with fluorescent paint and illuminated with ultraviolet light. An image of the sector of arc is formed in a plane containing the apex of a mirror surface wedge. The light striking the two surfaces of the wedge is reflected and illuminates the photocathode of the photomultiplier tubes. Rotation of the prism results in a displacement of the image and a consequent increase in the output of one tube and decrease in the output of the other.

Electronic filtering is provided to discriminate between the steady signal due to the ultraviolet excitation of the phosphor and any intermittent excitation due to strobe lamps to reduce any interaction between the level of light striking the phosphor and the error signal produced by the photomultipliers.

Four Chadwick-Helmuth Strobex lamps are flashed at the 16-frame-per-second camera rate to illuminate the separator and to stop the images of the protractors on the inner and outer races of the bearing so that angular position information is recorded on the photographs.

Four mercury vapor spot lamps with ultraviolet filters illuminate the flourescent patch for the tracking system.

The camera used was a Neyhart Enterprises model G-4. The camera film magazine accepts 100 or 200 foot reels of 35mm film. The camera has a data box, the image of which is projected onto each film frame.

IV Test Bearings

Three bearings were used in the roller to separator contact force investigation. They were mainshaft roller bearings representative of those used in aircraft gas turbine engines. Two of the bearings were 118mm bore, part number PWA 541043D, with cylindrical outer raceways. The third was 115mm bore, part number PWA 501511B with an out-of-round outer raceway. Dimensions and other characteristics of these bearings are given in Table 1.

V Separator Force Transducer

A roller contact force transducer was constructed on the bearing separator by introducing a cantilever beam between two of the bearing rollers. The cantilever beam replaced a rigid separating element so that cantilever beam deflection would give an indication of the roller contact force. A hole was drilled through one of the side rails of the separator to hold the fixed end of the cantilever beam. A notch to frame the deflected end of the cantilever was cut in the other side rail opposite the hole. Various beam cross-sections were used depending on contact forces and deflections encountered. A plastic rubbing block was cemented to the center portion of the beam to make up the normal roller spacing dimension of the rigid separator element replaced by the roller force indicating beam. A

duplicate modification was installed at 180° to the first to maintain separator balance.

With the shaft and test bearing operating at a speed and load condition to be investigated, the derotation prism was synchronized with the separator to produce a stationary image of the deflecting end of the cantilever beam as the roller and separator repeatedly moved through loaded and unloaded regions of the bearing. The 16 frame per second 35 mm instrumentation camera photographed the motions of the cantilever beam deflections relative to the notch in the separator. As roller contact forces may be expected to be a repetitive event from revolution to revolution the relatively slow framing rate can be extended to a very high effective framing rate by taking a large number of photographs over many revolutions of the bearing. This gives frames covering 0 to 360° to the applied load. The angle to the applied load was indicated by the position of the cantilever beam relative to a fixed protractor on the bearing outer race. Radial loads were applied vertically at the 360 (0) degree mark on the protractor.

VI Force Transducer Calibration

The force transducing cantilever beam was assembled into the separator with epoxy resin with the plastic spacing element also epoxied in place. The separator was held in a small vise and loaded with a wire hook positioned over the plastic rub block. A small weight pan and weights were used to load the cantilever beam. Cantilever deflections were photographed. Figure 2 shows a representative force-deflection relation.

VII Experimental Procedure

The lubricating oil used throughout the tests was a 5-centistoke neopentylpolyol (tetra) ester. This is a type II oil which conforms

to specification MIL-L-23699. Test bearing inlet oil was heated and controlled to 485° K (150°F).

The Separator Study Machine bearing rig was started with a load applied and brought up to speed, the desired load condition applied, the prism synchronized with the separator and 100 to 200 photographs taken. Film used was Kodak 2475 Recording Film. It was cut into lengths fitting stainless steel reels and developed in a small tank with HC 110 developer, dilution A, for 30 minutes at laboratory room temperature. This seemed to give images of adequate contrast, with background fog just beginning to be noticeable on fresh film.

VIII Data Analysis

After chemical processing of the film was completed the film was respliced and read with a Benson-Lehner model N-2 film reader capable of indicating 4 digits with the least digit representing 0.005 mm (0.0002 in.) in the film image. The film images, however, varied in density and sharpness from frame to frame due to variation in Xenon flash intensity, duration, and jitter in flash initiation among the four Xenon flash tubes.

Readings were taken by aligning a cross-hair onto the lowest edge of the notch for R1, the bottom of the beam end for R2, the top of the beam end for R3, and the top of the notch for R4. A computer program was used to calculate differences R2-R1, R3-R1, R4-R1, R3-R2, R4-R3, and R4-R2. From R4-R1 and R3-R2 a consistency check was available to pull out or correct obviously defective readings as the notch dimension and beam height should always be of constant value. After subtraction of undeflected (zero) readings, the differences give indications of the beam deflection in that film frame.

The computer program also calculated average values of notch size for the photo set and normalized the deflection indications on the average notch size to compensate for image size variation with focus setting. The program scaled the deflections to the lineal measured notch dimension. The deflection indications were then multiplied by the spring constant determined in the force transducer calibration, and the resulting case forces are listed and plotted by a Calcomp plotter.

It was possible to determine cage to shaft speed ratio with some accuracy over 10 successive photographs of multiple shaft revolutions from the following considerations.

As stated previously, the derotating prism is synchronized to rotate at half the separator speed thus producing a stationary image of the separator to be photographed. Protractors which are mounted on the stationary outer race and on the rotating inner race are visible in the photographs. Four Xenon flash tubes with a flash duration of 50 microseconds permit clear instantaneous photographs of the stationary separator and stop the motion of the protractor images. Typically 100 to 200 photographs were taken at a cine frame rate of 16 per second for each case investigated.

In these photographs the angle turned through by the separator (cage) can be determined from the difference in angle on the stationary outer race protractor between two consecutive frames. Thus,

$$2\Delta\theta_p = \Delta\theta_c = \Delta\theta_o = \left(\frac{W_c}{W_s}\right) W_s \Delta t \qquad (1)$$

where:

$\Delta\theta_p$ = true prism angle turned through

$\Delta\theta_c$ = true cage angle turned through

$\Delta\theta_o$ = angle difference $+360^\circ$ x number of revolutions between photographs

$\frac{W_c}{W_s}$ = separator to shaft speed ratio in the operating bearing

W_s = shaft speed

Δt = time between photographs

The protractors are engraved with angle increasing in the direction of shaft rotation. The shaft turns through a greater angle than does the separator; consequently, the cage photographs centered on the transducer in the cage show the inner race angles decreasing. The true angle that the shaft has turned through in the 1/16 second between successive frames may be determined from the protractor angles photographed by

$$\Delta\theta_s = \Delta\theta_o - \Delta\theta_{st} = \left(\frac{W_c}{W_s}\right) W_s \Delta t - W_s \Delta t \qquad (2)$$

where:

$\Delta\theta_s$ = angle difference on inner race protractor between photographs

($\theta_{s_{i+1}} - \theta_{s_i}$ with i being the frame number)

$\Delta\theta_{st}$ = true angle turned through by the shaft in time Δt

From equation 2, then $\Delta\theta_{st} = \Delta\theta_o - \Delta\theta_s$, and $W_c \Delta t = \Delta\theta_o$, $W_s \Delta t = \Delta\theta_{st}$ so:

$$\frac{W_c}{W_s} = \frac{\Delta\theta_o}{\Delta\theta_o - \Delta\theta_s} \qquad (3)$$

where $\Delta\theta_s$ is a negative number.

Care must be taken in calculating angle differences $\Delta\theta_o$ and $\Delta\theta_s$ between photographs and in using equation (3). Multiple revolutions of shaft and separator occur without this being apparent in the photographs. At 16 frames per second with an appropriate epicyclic speed for W_c/W_s the ranges of angle differences given in Table 3 may be anticipated.

To obtain the true angle of rotation of the cage between successive frames, it is necessary to:

1. Subtract the angle read from the reference point of the separator in the photograph from that read in the i-1 frame.
2. Determine the number of full rotations between frames using Table 4.
3. Add the number of full rotations to the difference found in step 1.
4. Critically examine the value calculated if the test speed is close to a speed at which a different number of revolutions might be possible or if speeds much different from epicyclic might occur.

These considerations led to the cage/shaft speed ratios that appear on the cage force figure captions and in the cage/shaft speed ratio versus load figures.

IX Results and Discussion

This investigation was undertaken to experimentally evaluate roller to cage contact forces. It was subsequently noted that information on cage to inner race land contact force, and cage to shaft speed ratios was also available in the data obtained.

A. Roller to Cage Contact Forces

The principal results of this investigation are the roller to cage contact forces shown in Figures 3-5. These figures show the roller force on the cage as a function of roller location in the bearing. Roller location is measured clockwise from the centerline of the radial load at 0^{o} (360^{o}). Table 2 summarizes the data obtained.

Different spring constants were necessary as the investigation progressed and as larger forces were encountered. The investigation began with a spring constant of 22.8 N/mm (130 lb/in). These transducers appeared to function adequately in the 501511B bearing with the out-of-round outer raceway, and were initially installed in the 541043D-1 bearing with the 0.18 mm (0.0073 in) clearance. Failures in bending fatigue occurred in beams with 22.8 N/mm (130 lb/in) and 29.3 N/mm (160 lb/in) spring constants.

Transducers of spring constant 75.9 N/mm (454 lb/in) were fabricated and used in the 541043D bearings to obtain the data of Figures 3a-i and 4a-i.

Positive forces in the figures are those exerted by rollers tending to accelerate the cage. Negative forces are those exerted by rollers tending to retard or decelerate the cage. In general stiffer cantilever beam deflecting elements indicate greater forces, with more scatter in the film readings.

The force indicated by a cantilever deflection is created by a roller advancing into the cantilever located on the cage. A roller's advance relative to the cage, which moves with average roller speed, is determined by roller kinematics such as roller location on the raceway path, deflections, etc. The motion of the roller relative to the average roller

will deflect the cantilever until the roller begins to recede from the cantilever due to roller kinematics, provided limiting traction forces are not exceeded. Thus the cantilever is deflected as much as necessary to accomodate the roller advance relative to the cage. For a given roller advance, the stiffer cantilever's deflection indicates larger force. The stiffer cantilever deflecting elements will also have smaller deflections. Errors in measuring the stiffer cantilevers' deflections will produce larger variations in the force measurements. All of the variation in the figures may not be due to errors in cantilever deflection, however. It is possible that there is some variation in the rollers' motion as they traverse various portions of raceway surfaces with possible cage motions of oscillation, rocking and impacting on rollers and inner race land surfaces.

Loads of 360, 670, 1330, and 4450 N (80, 150, 300, and 1000 lb) were applied to the 501511 B bearing without indication of skidding. When these same loads were applied to the 541043 D-1 bearing the cage to shaft speed ratios were 0.396, 0.409, 0.438, and 0.453 at 4,000 rpm as compared to the 0.4562 epicyclic speed ratio. Loads of 6670, 4450, and 2220 N (1500, 1000, and 500 lb) were used in the rest of the investigation to reduce the likelihood of skidding damage to the test bearings. The percent slip for these bearings is given in Table 2.

Figures 3 and 4 show the magnitude and distribution of roller to cage forces in the 0.18 mm (0.0073 in) and 0.21 mm (0.0083 in) clearance bearings as indicated by a 79.5 N/mm (454 lb/in) spring constant transducer. The 0.18 mm clearance bearing seems to experience a rather narrow but well defined force peak of 40 N (9 lb) in lightly loaded high speed cases which is not apparent in the 0.21 mm clearance bearing data, though other

general characteristics of the two bearings are similar in that positive and negative forces of 25 N (5 lb) are not uncommon at 8,000 and 12,000 rpm speeds.

Figure 5 seems to indicate that the cage of the out-of-round outer race bearing experiences forces of 5 to 10 N (1 to 2 lb) that are more nearly constant throughout the bearing. These data were obtained with a 22.8 N/mm (130 lb/in) transducer. Testing with this bearing was terminated after severe fretting was discovered. This was apparently due to centrifugal force loosening the fit between the bearing, sleeve spacer, and shaft of the test rig. The sleeve for the 118 mm bearings was manufactured to provide a 0.025 mm (0.001 in) interference at the shaft diameter after the sleeve was assembled in the bearing bore, and has seemed to function adequately.

B. Cage to Inner Race Land Contact Force

From the data of Figures 3,4, and 5 it was possible to derive the force between the cage and its guiding contact with the inner race land. This force was obtained by taking horizontal and vertical components of each force point as plotted in Figures 3,4, and 5. Adding vertical and horizontal forces in a 12.9 degree sector, and dividing by the number of forces in the sector gave the average force one of the 28 rollers would exert on the cage. The sum of the 28 roller forces should equal the resultant force that the inner race must exert on the cage. The angular location of the resultant force was obtained by taking the arc tangent of the ratio of horizontal to vertical force components. Figure 6 summarizes the magnitude and direction of the cage to inner race land force due to ball contact forces for various speeds and loads. It should be noted that this calculation did not include the weight of the cage (1.63 and 2.24 N (0.37 and 0.50 lb) for the 118 and 115 mm bearings).

C. Cage to Shaft Speed Ratios

Figure 7 shows the cage to shaft speed ratios calculated by the method described in Section VIII, Data Analysis. The epicyclic cage speed for the 115 mm may be calculated from the data in Table 1 to be 0.4565 and that for the 118 mm bearing to be 0.4562. Figure 7 and Table 2 seem to indicate that the out-of-round outer raceway bearing had little tendency to skid, (0.2% cage slip) even at very low loads, while the cylindrical outer raceway bearings did skid appreciably at very low loads, and had a maximum value of cage to shaft speed ratio of 0.4539 (0.5% cage slip) for the larger clearance bearing at a 6670 N (1500 lb) load, the maximum used, at the 4,000 rpm speed.

X Summary of Results

Roller to cage contact forces were evaluated experimentally. The maximum roller-cage force observed was 43 N (9.5 lb) and occurred at light load and high speed. Resultant cage to shaft forces were calculated from roller to cage contact forces. The maximum cage-shaft force was 60 N (13.6 lb) and also occurred at light load and high speed. The out-of-round outer raceway was effective in preventing skidding even at very light loads. Skidding was observed, however, in the cylindrical outer race bearings.

XI References

1. Brown, P.F., "Bearings and Dampers for Advanced Jet Engines", Paper 700318 SAE National Air Transportation Meeting, New York, New York, April 20-23, 1970.

2. Gupta, P.K., Transient Ball Motion and Skid in Ball Bearings Journal of Lubrication Technology, Trans. ASME, Series F, Vol. 97, 1975, No. 2, pp 261,269.

3. Harris, T.A., "An Analytical Method to Predict Skidding in Thrust Loaded Angular Contact Ball Bearings", Journal of Lubrication Technology, Trans. ASME, Series F, Vol. 73, 1971, pp. 17-24.

4. Poplawski, J.V., "Slip and Cage Forces in A High Speed Roller Bearing", Journal of Lubrication Technology, Trans. ASME, Series F, Vol. 72, pp.

5. Walters, C.T., "The Dynamics of Ball Bearings", Journal of Lubrication Technology, Trans. ASME, Series F, Vol. 93, 1971, pp. 1-10.

6. Signer, H.R., "Experimental Ball Bearing Dynamics Study", NASA CR 134528, October 1973.

7. Nypan, L.J., "Ball to Separator Contact Forces in Angular Contact Ball Bearings Under Thrust and Radial Loads," NASA CR-2976, April 1978.

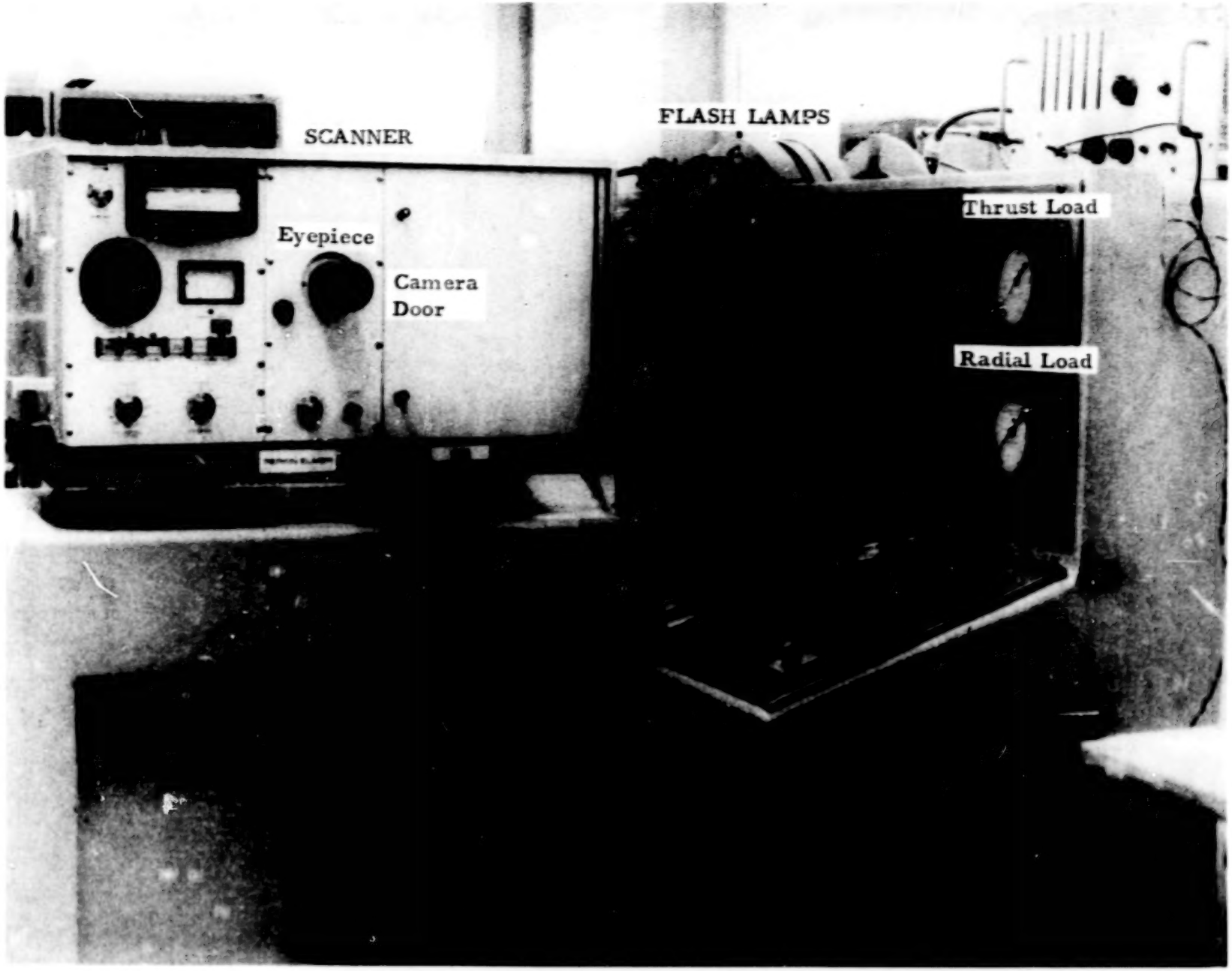

FIG. 1a Separator Study Machine

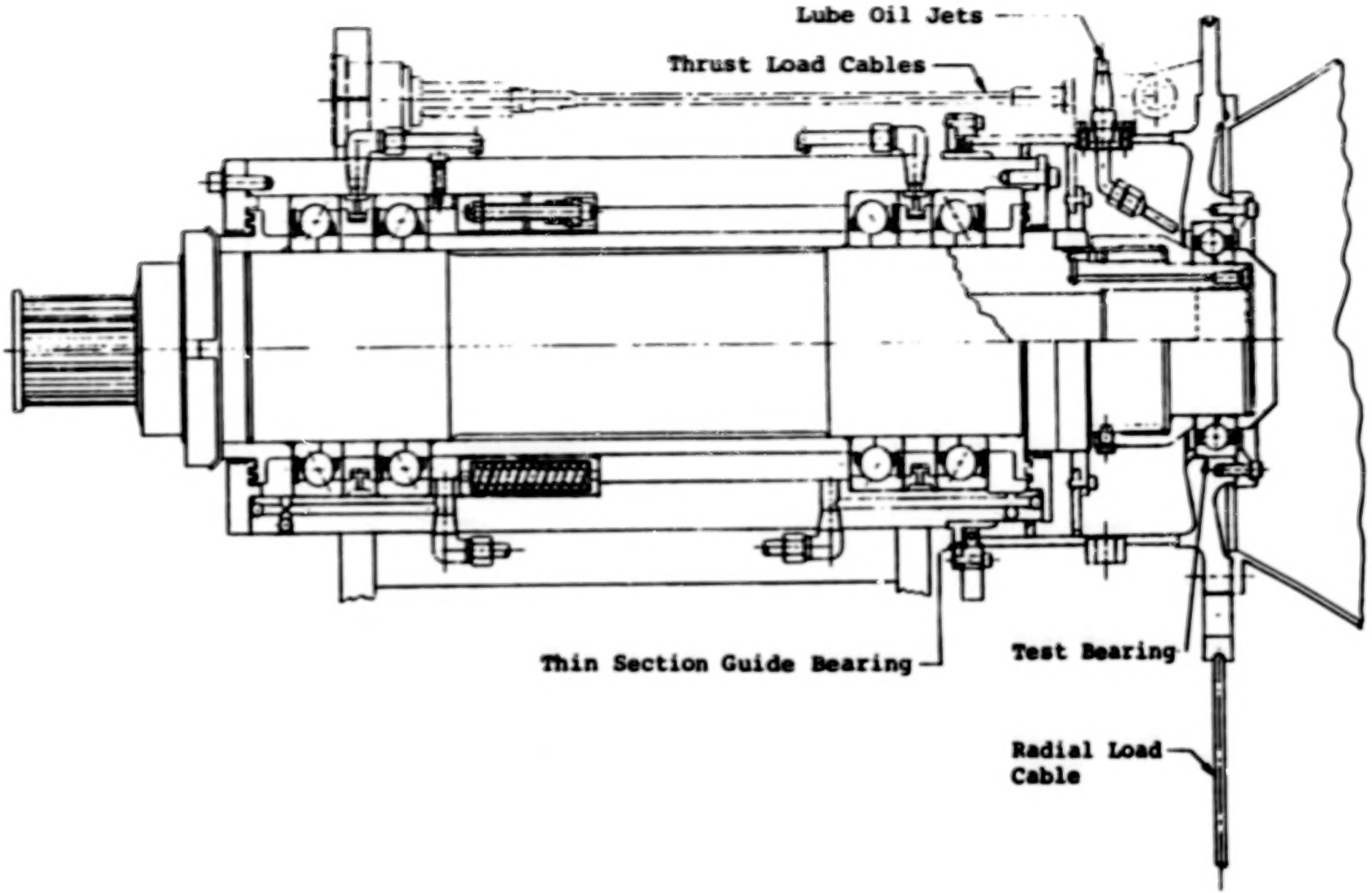

FIG. 1b Schematic of Shaft Assembly

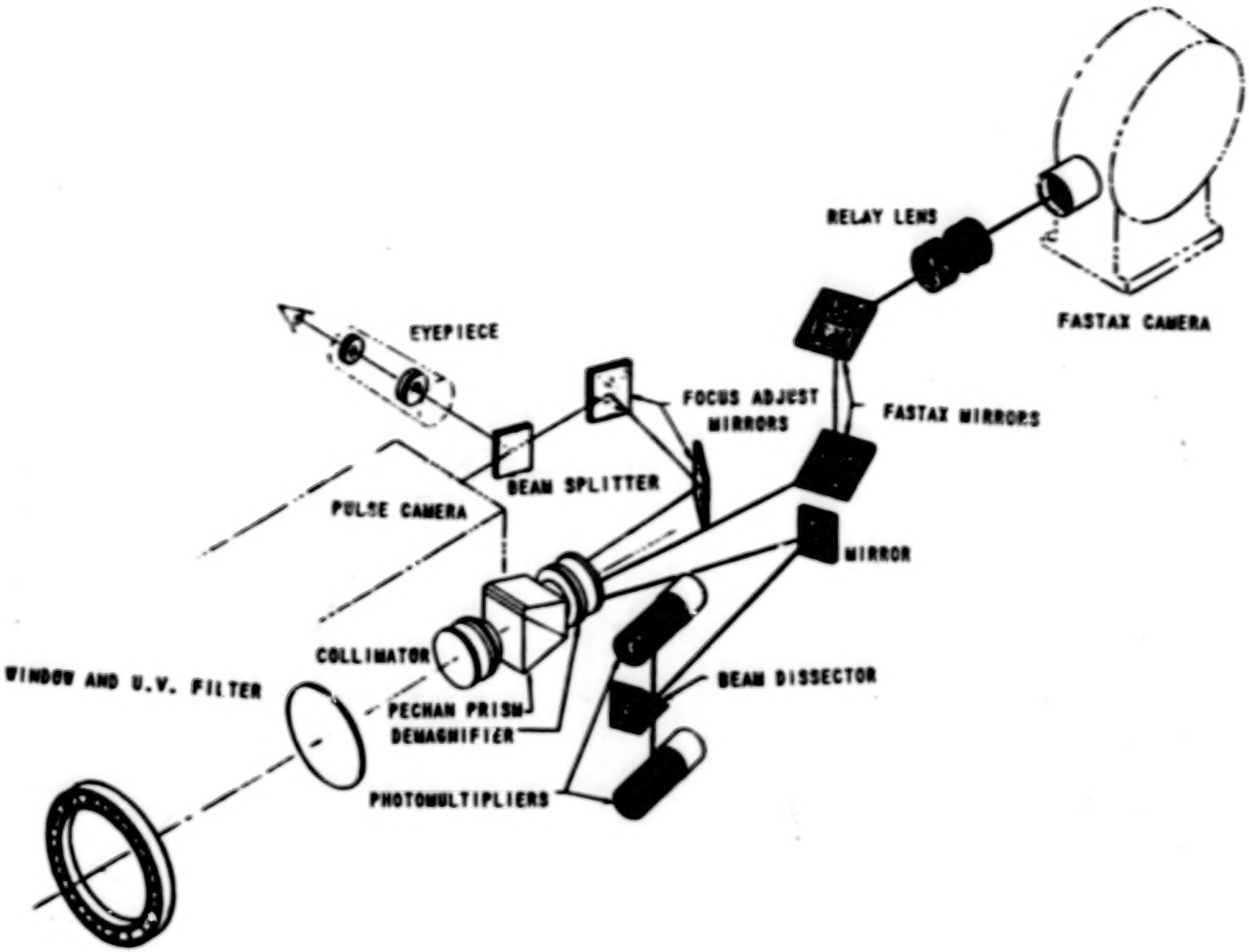

FIG. 1c Light Paths Through the Scanner

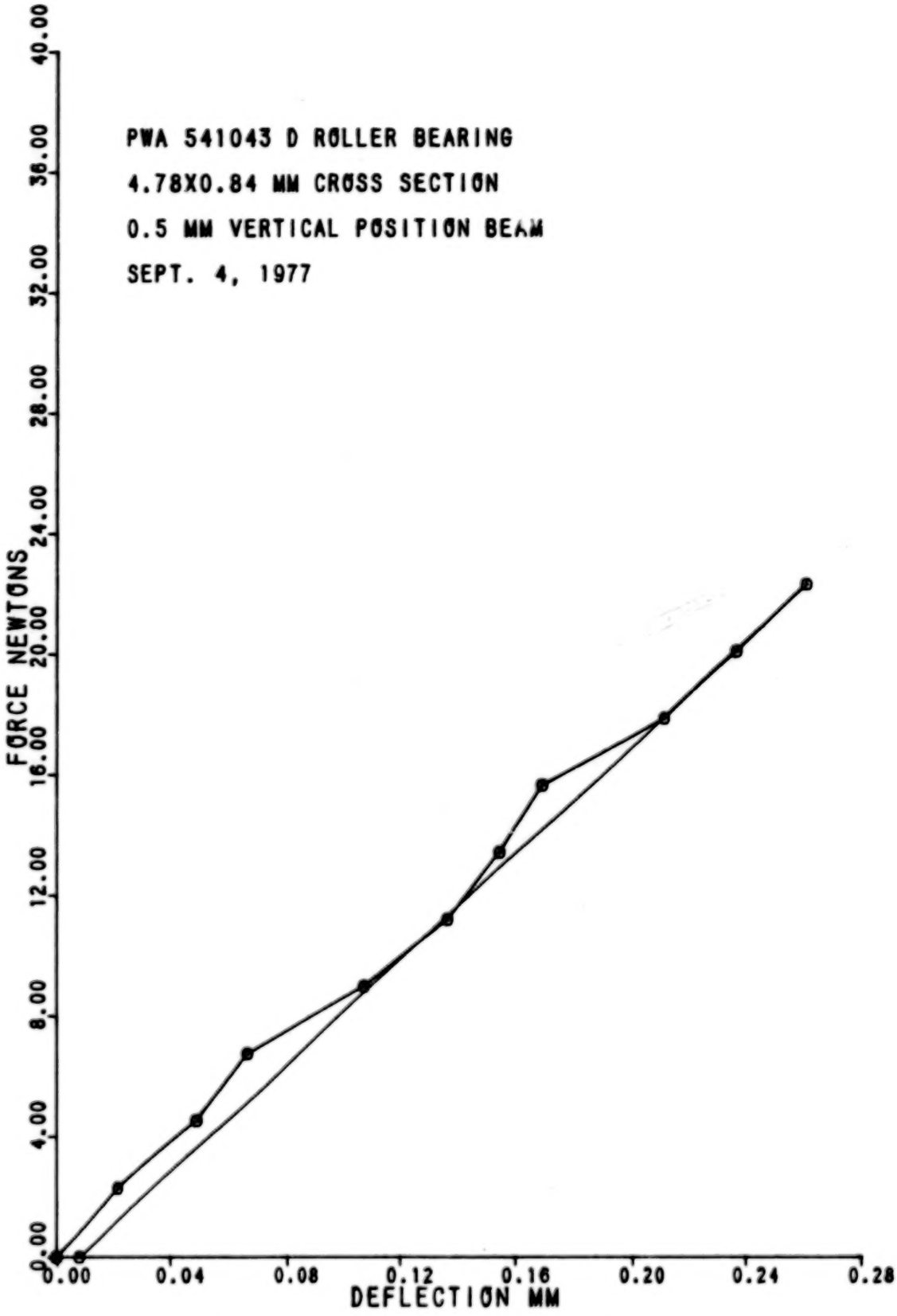

FIG. 2 Sample Force Transducer Calibration

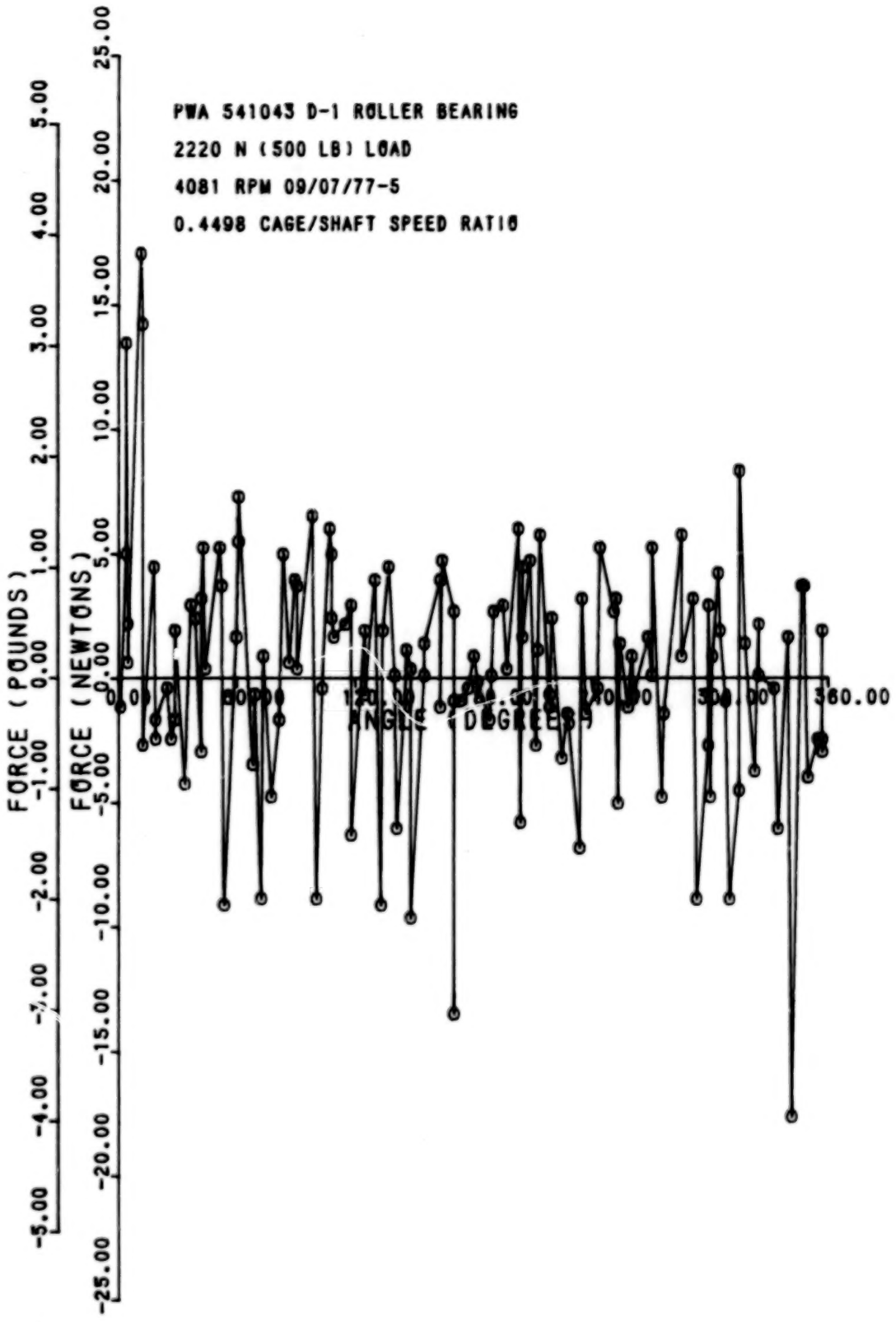

FIG. 3a Roller Contact Forces 0.18 mm Clearance Bearing

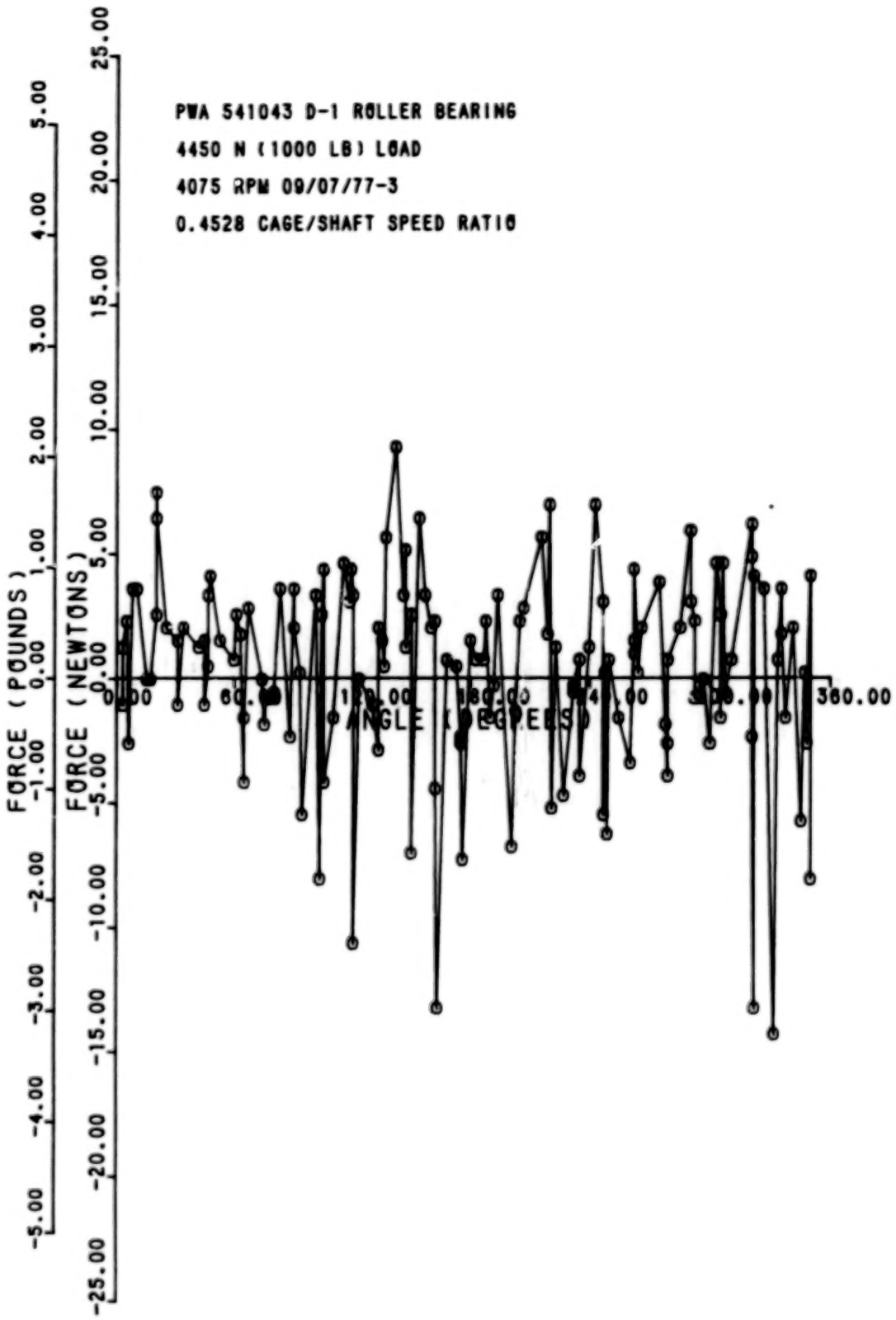

FIG. 3b Roller Contact Forces 0.18 mm Clearance Bearing

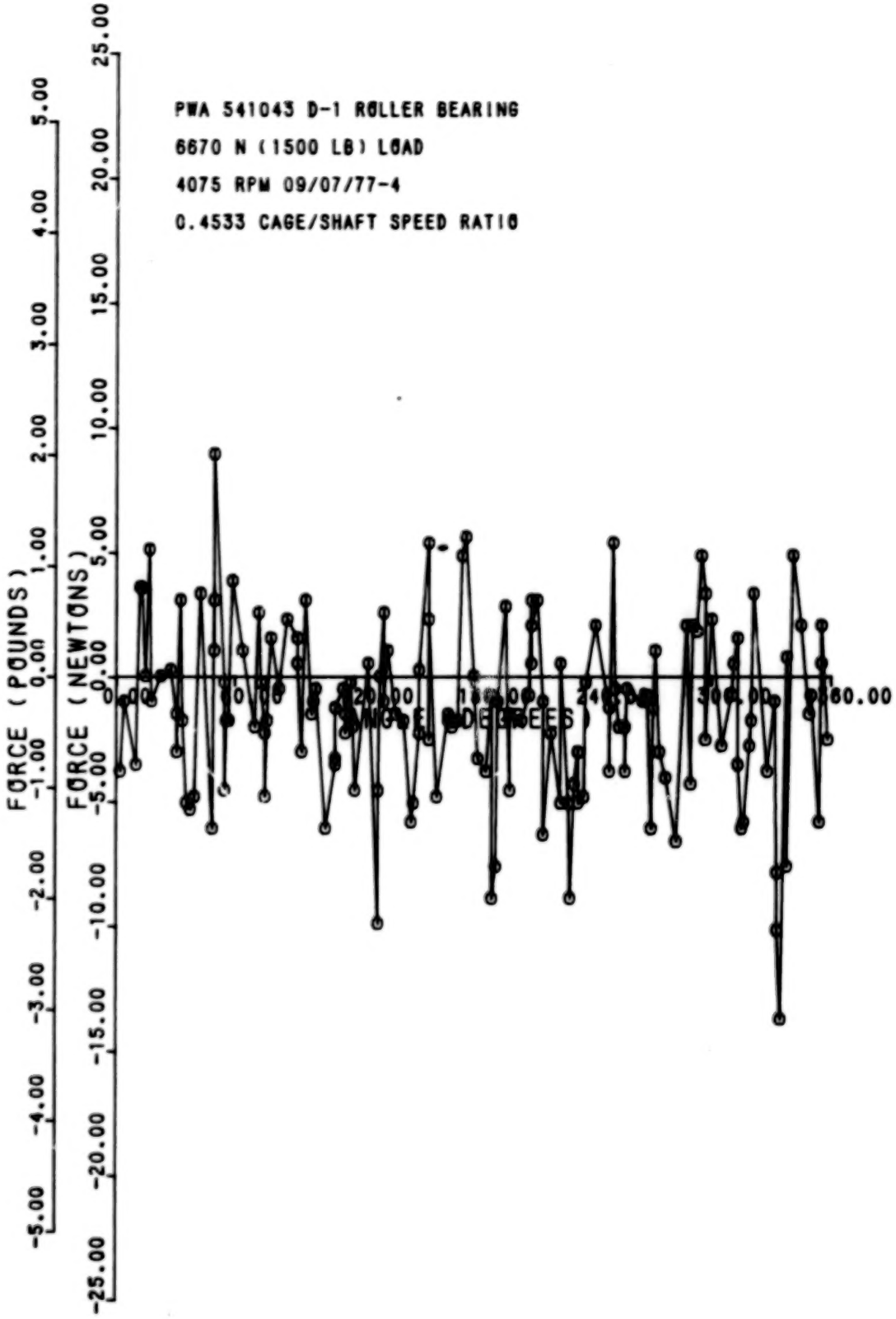

FIG. 3c Roller Contact Forces 0.18 mm Clearance Bearing

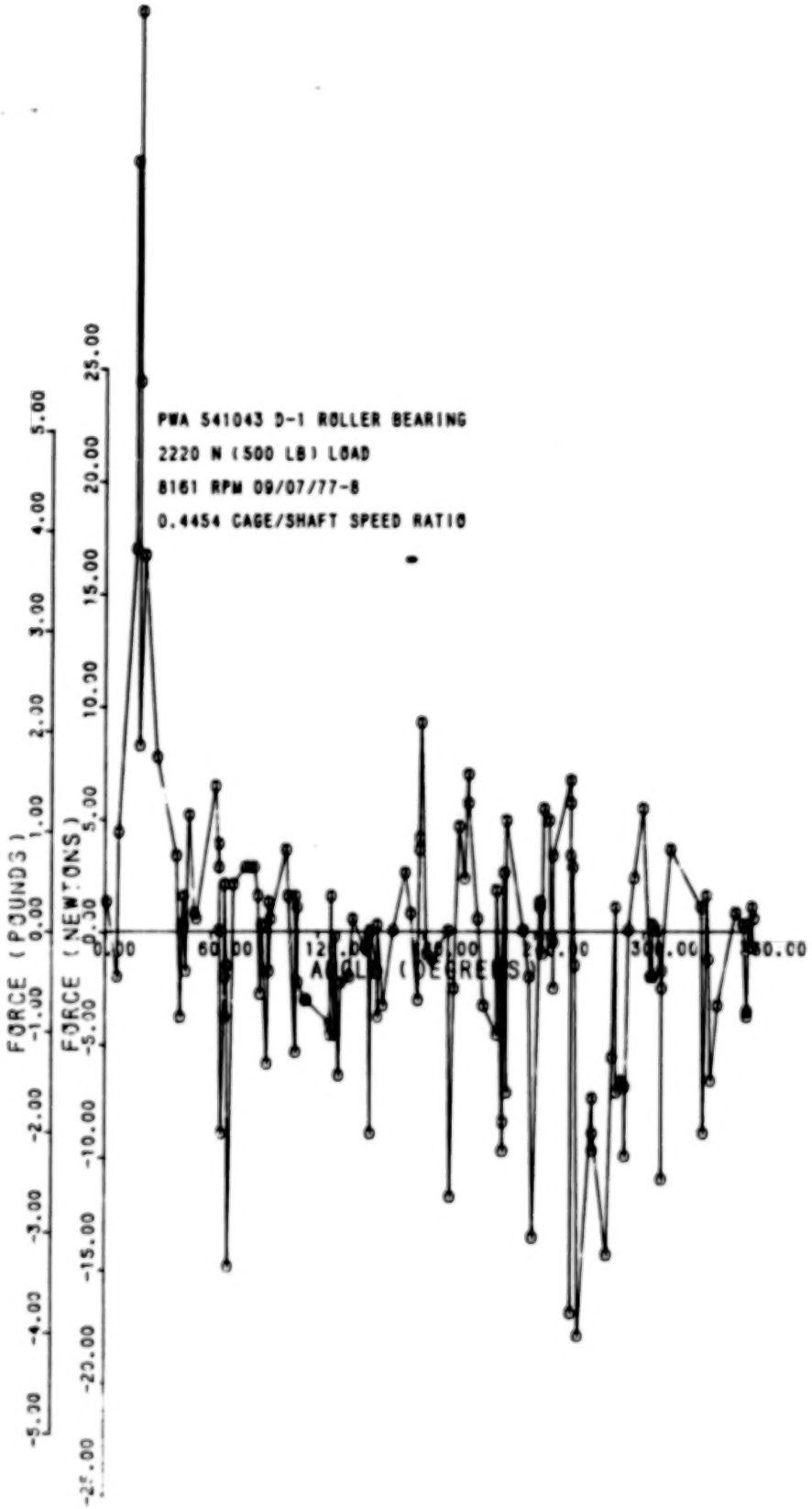

FIG. 3d Roller Contact Forces 0.18 mm Clearance Bearing

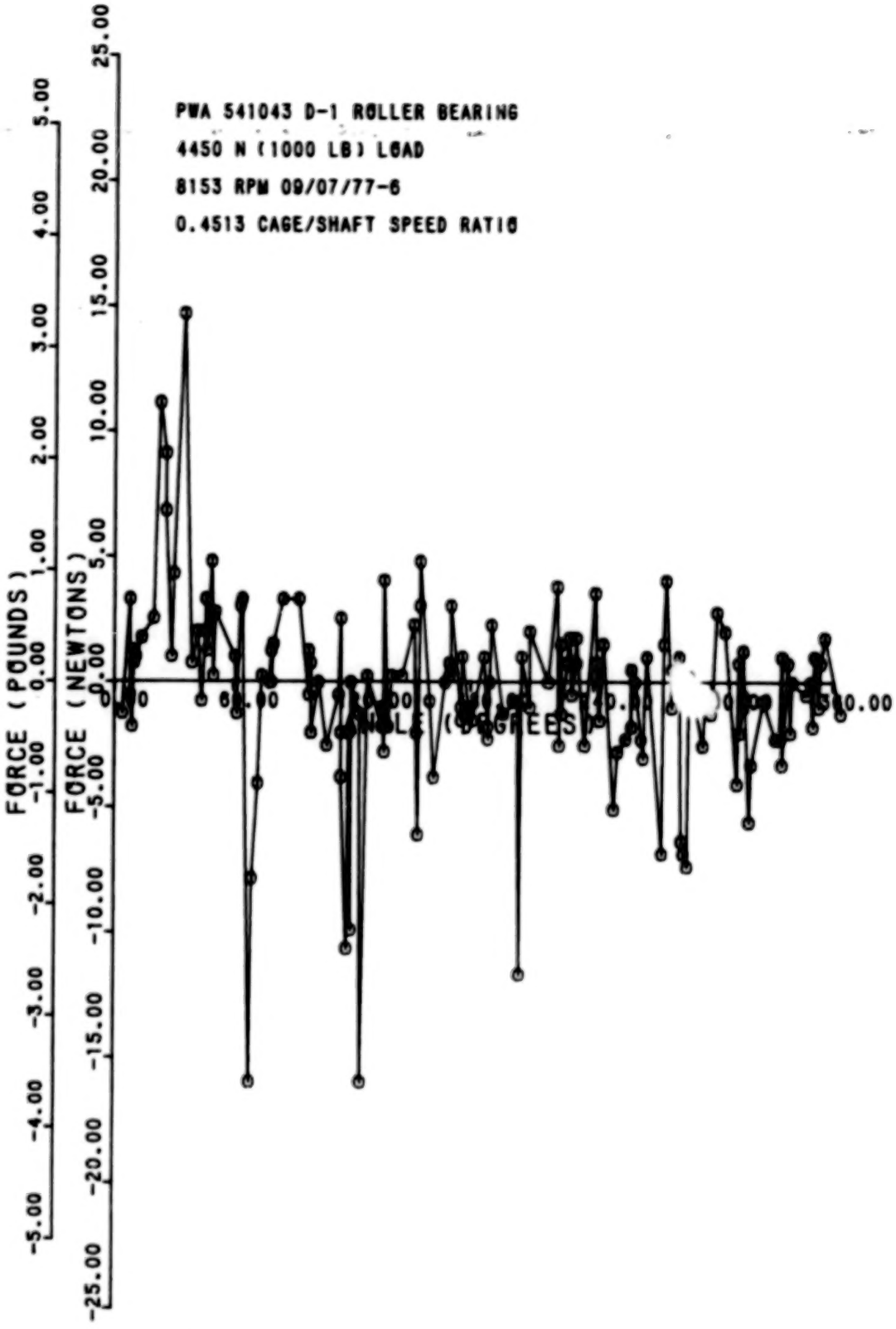

FIG. 3e Roller Contact Forces 0.18 mm Clearance Bearing

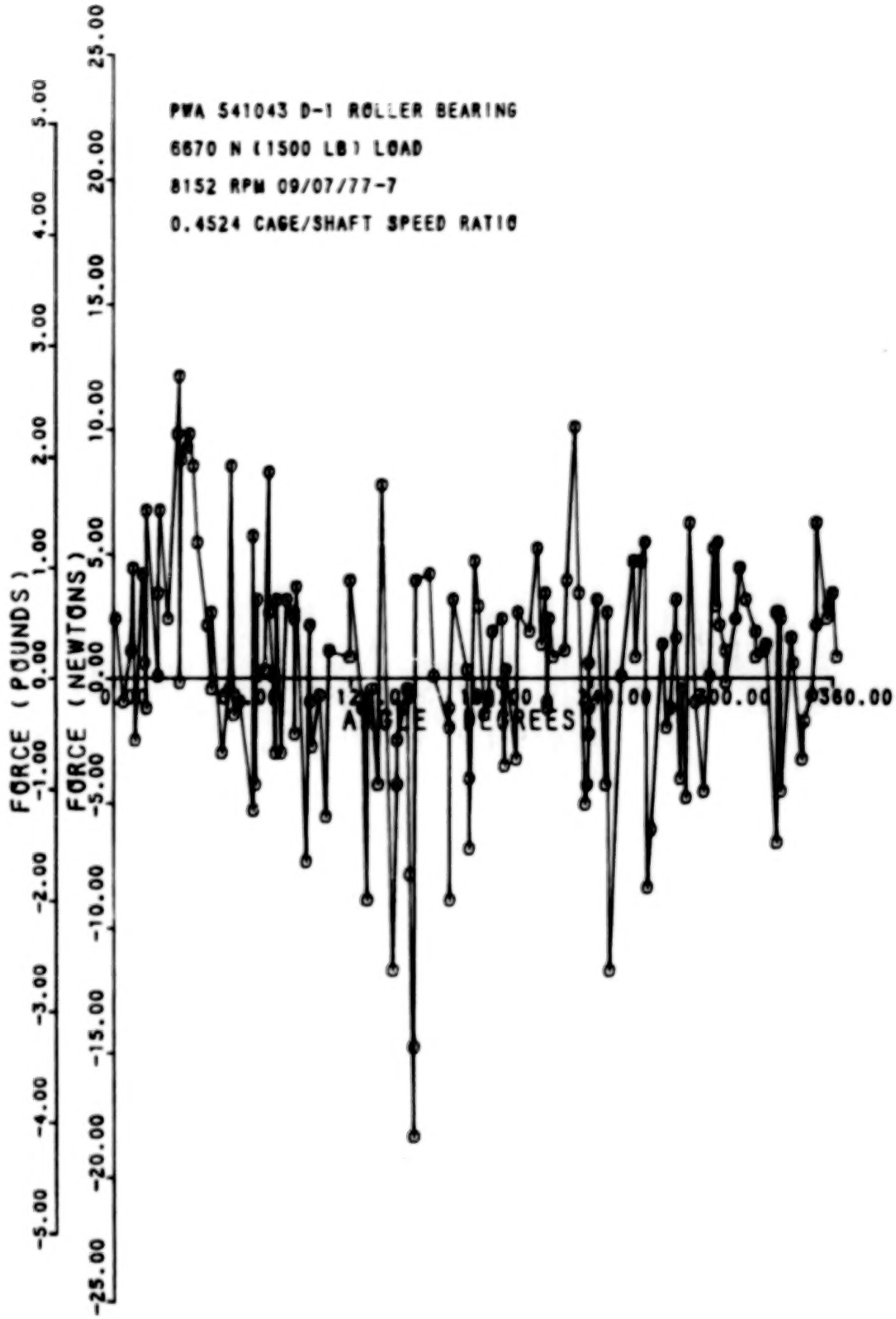

FIG. 3f Roller Contact Forces 0.18 mm Clearance Bearing

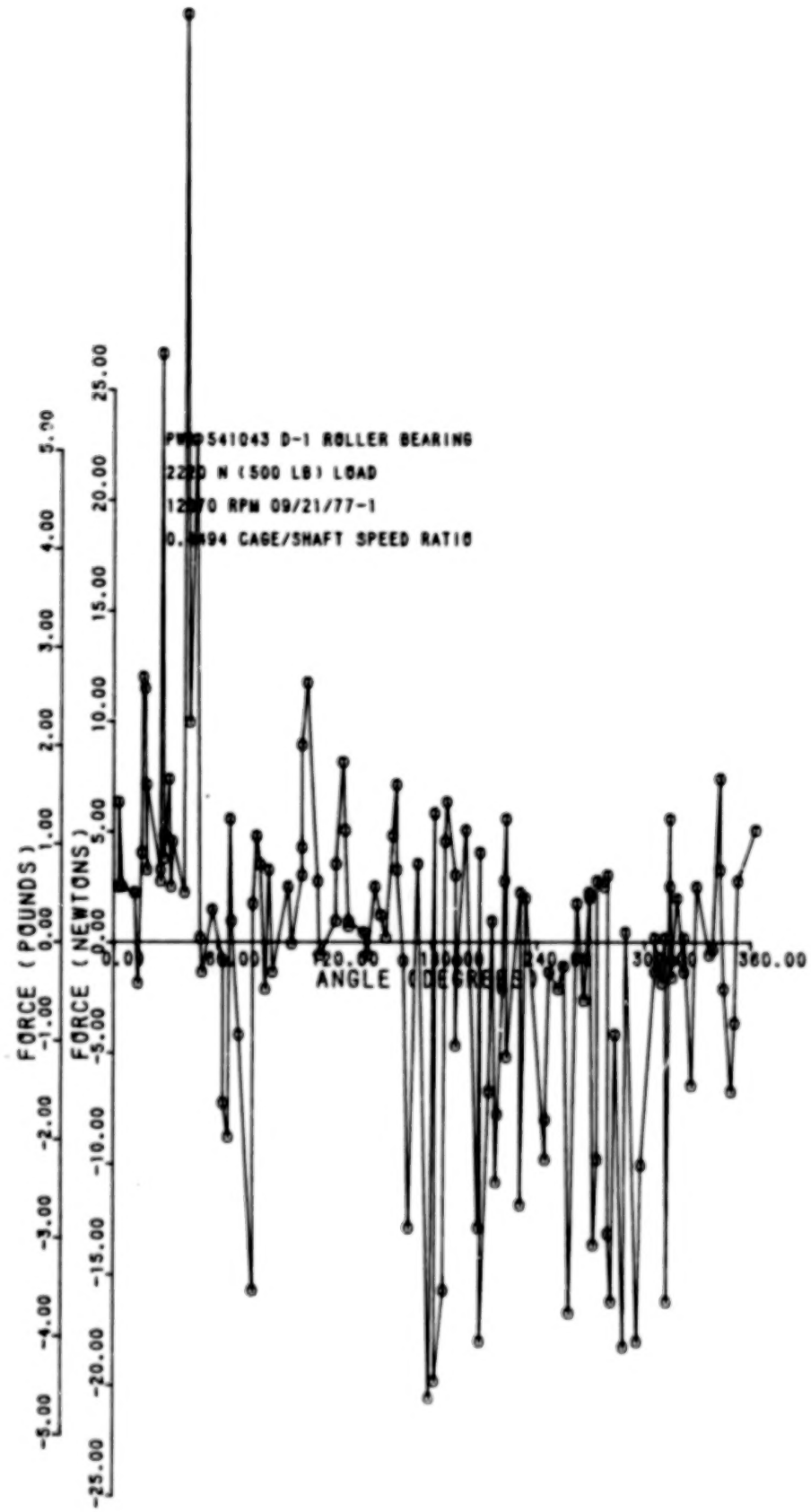

FIG. 3g Roller Contact Forces 0.18 mm Clearance Bearing

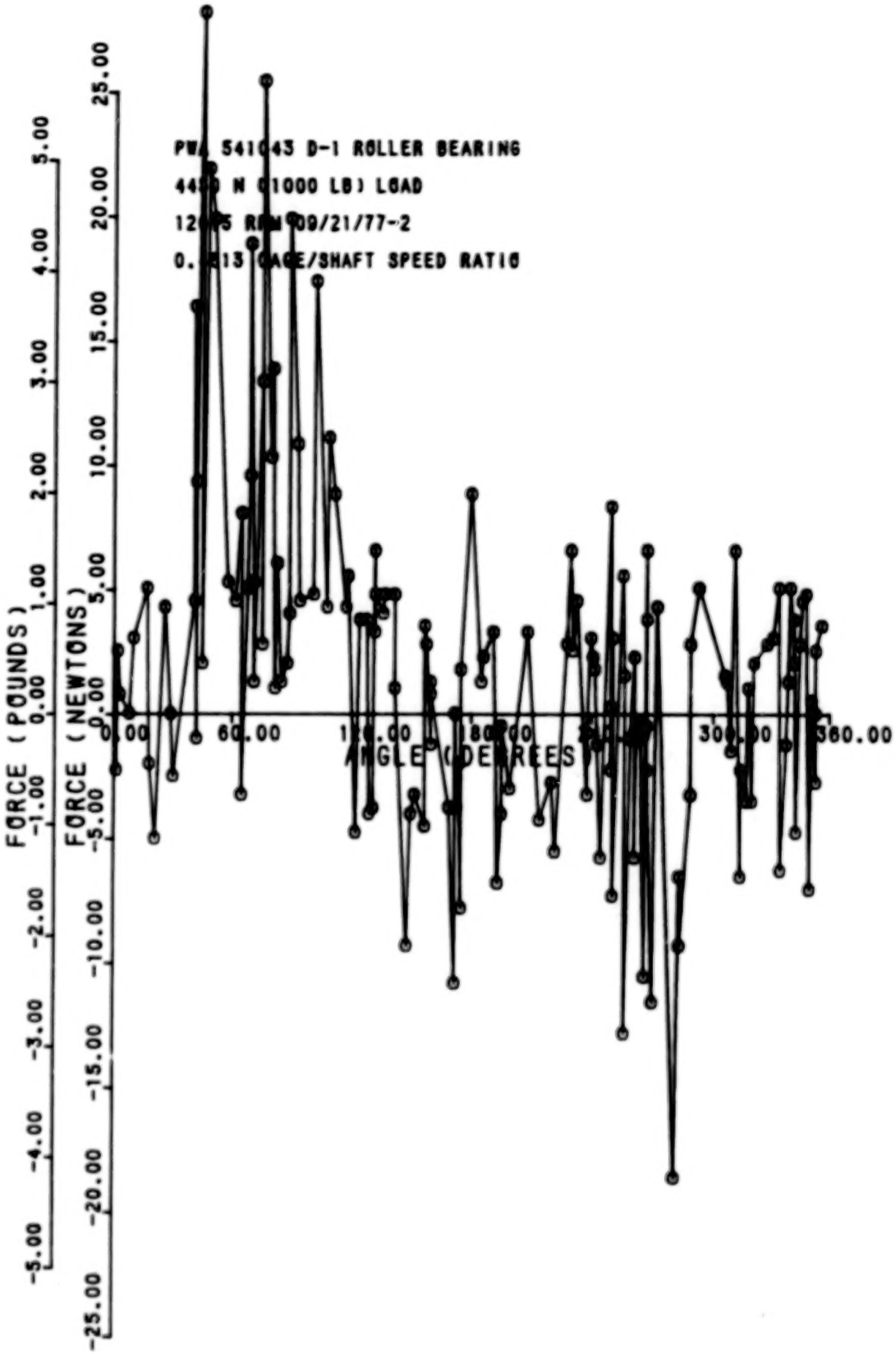

FIG. 3h Roller Contact Forces 0.18 mm Clearance Bearing

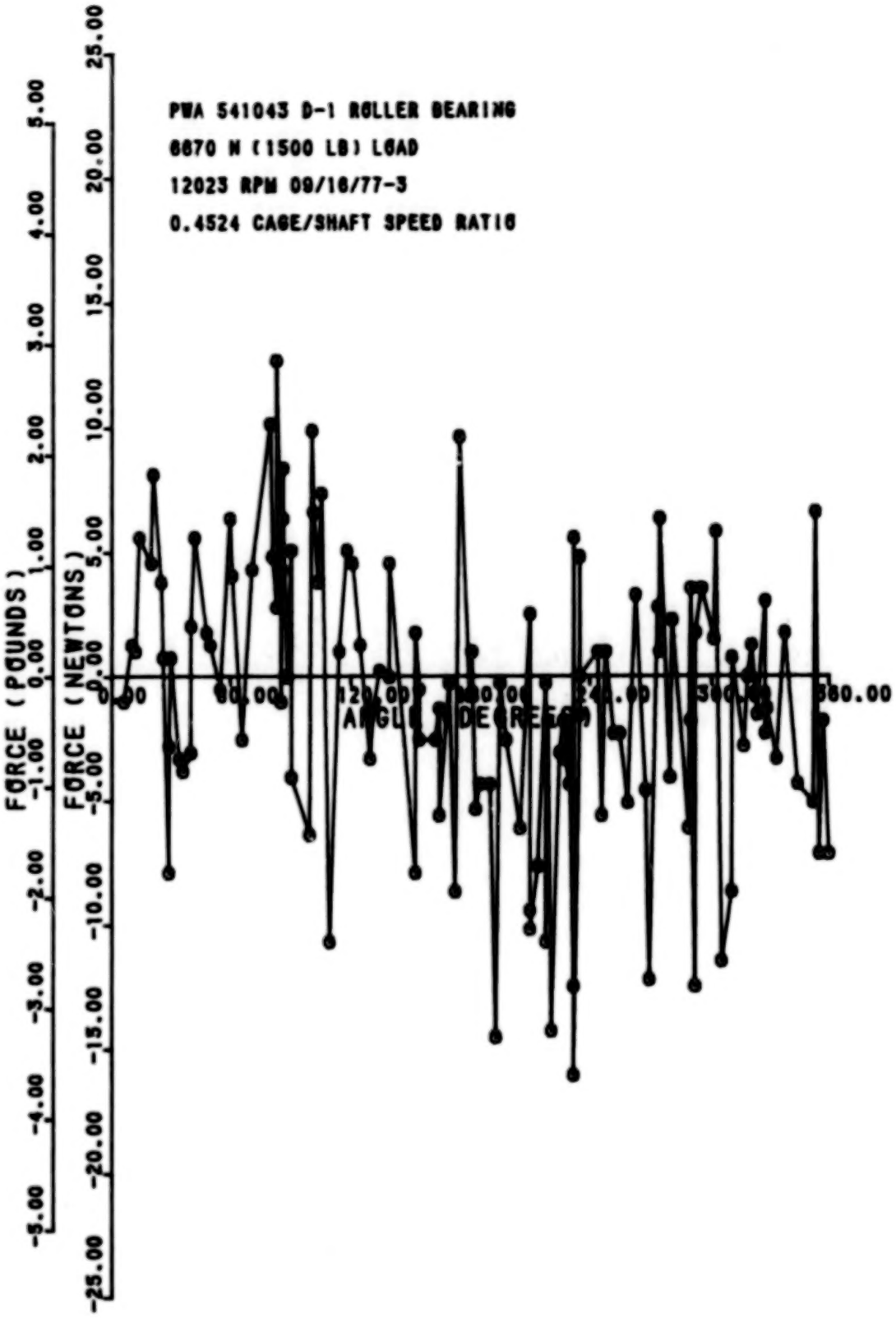

FIG. 3i Roller Contact Forces 0.18 mm Clearance Bearing

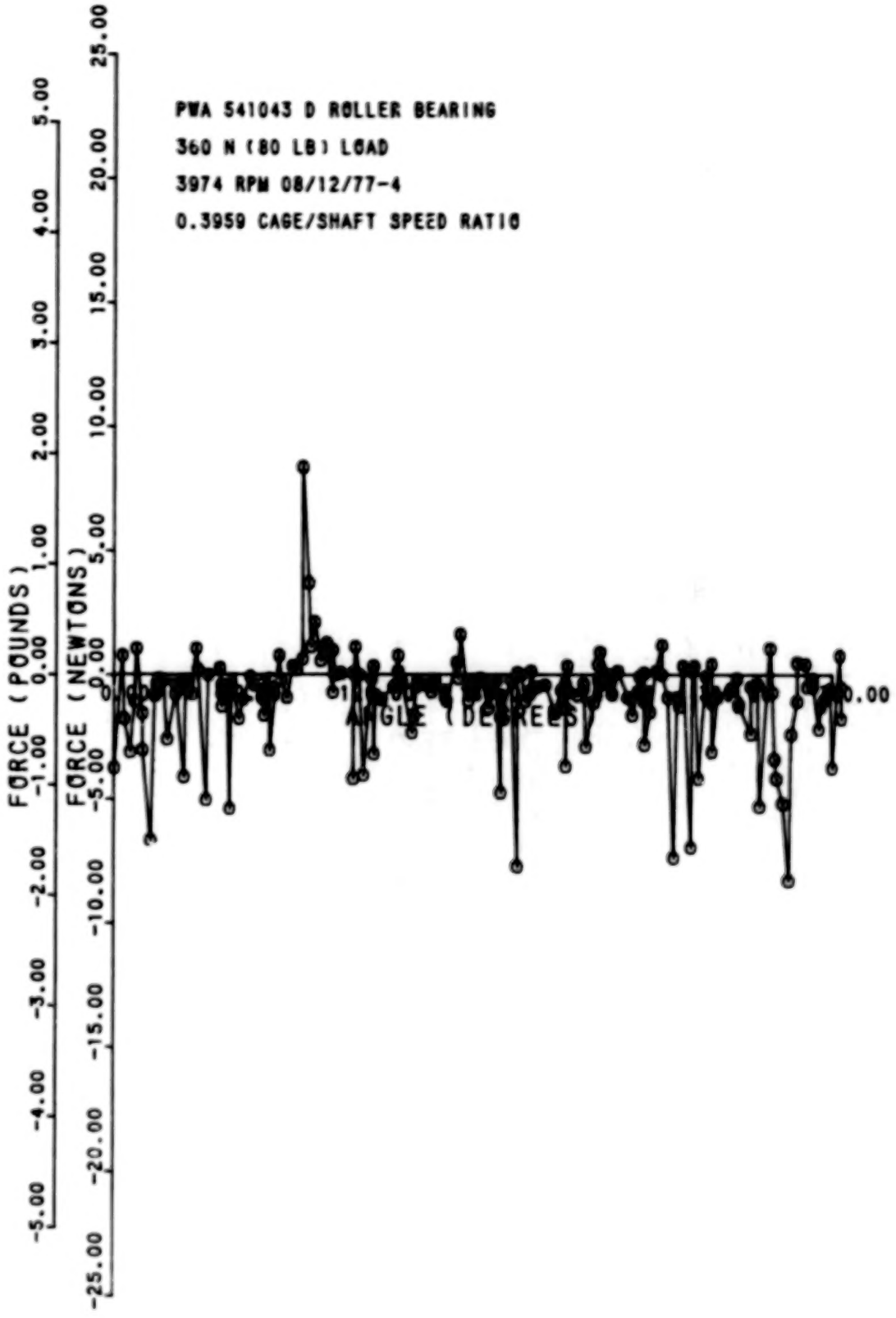

FIG. 3j Roller Contact Forces 0.18 mm Clearance Bearing

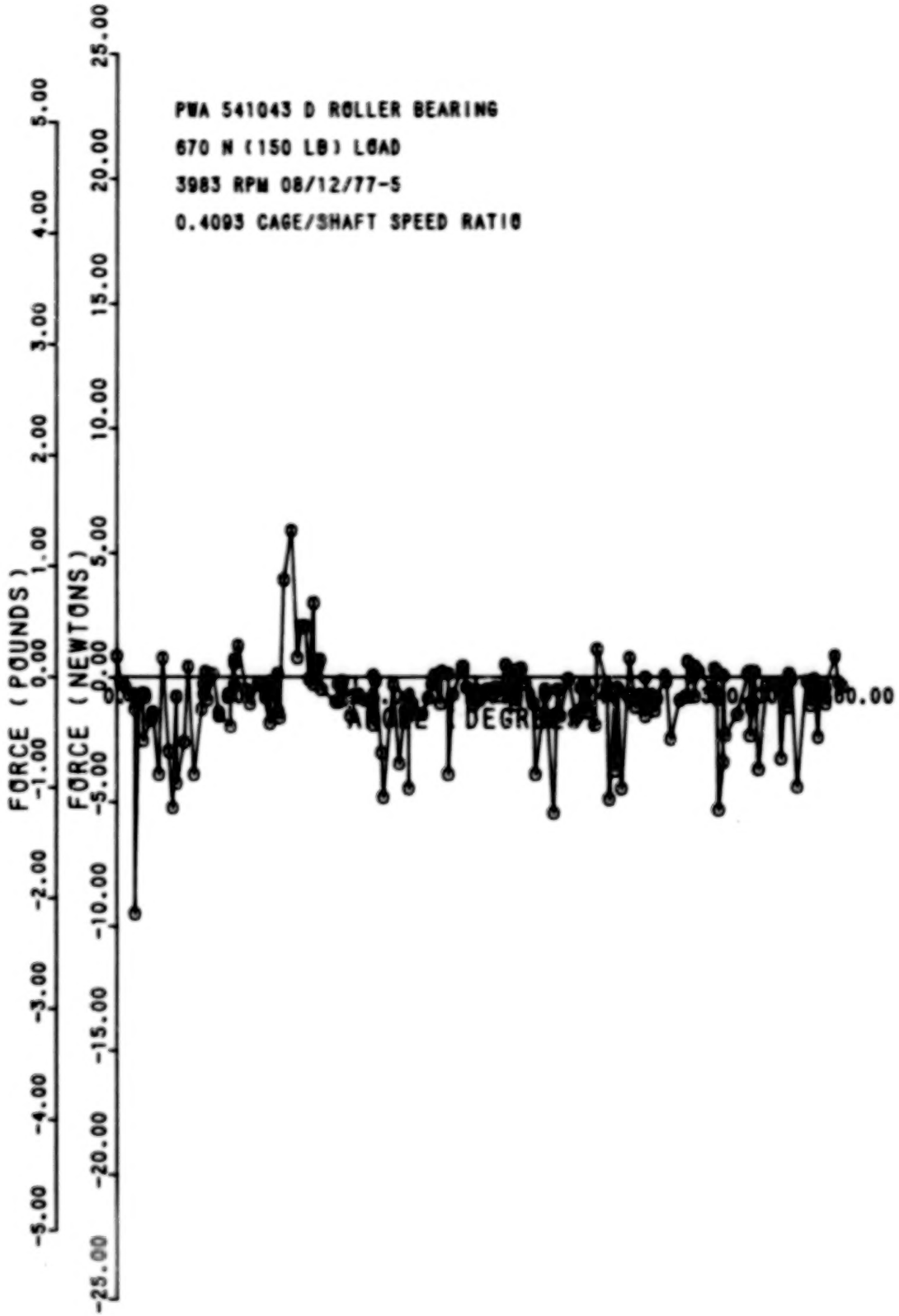

FIG. 3k Roller Contact Forces 0.18 mm Clearance Bearing

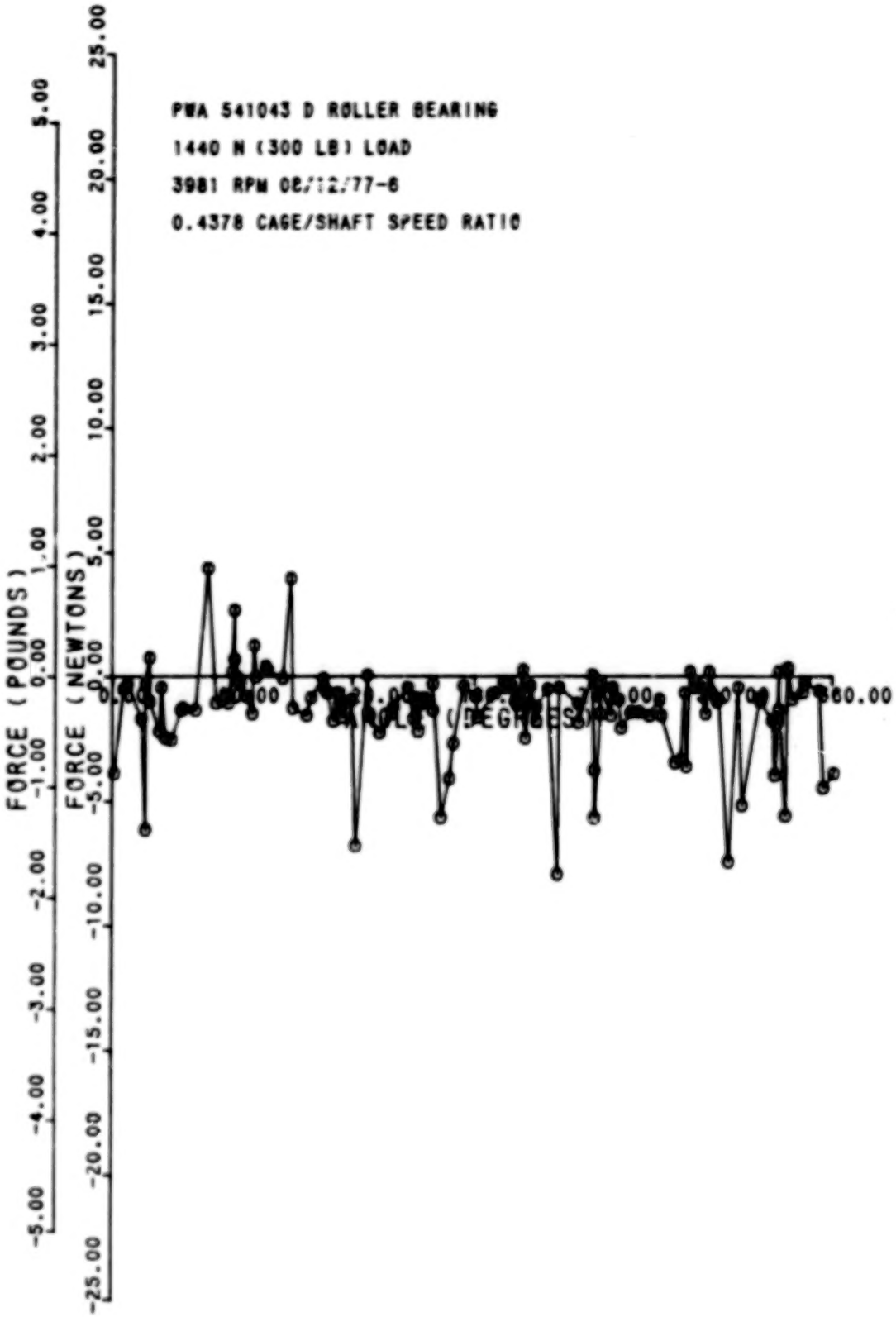

FIG. 31 Roller Contact Forces 0.18 mm Clearance Bearing

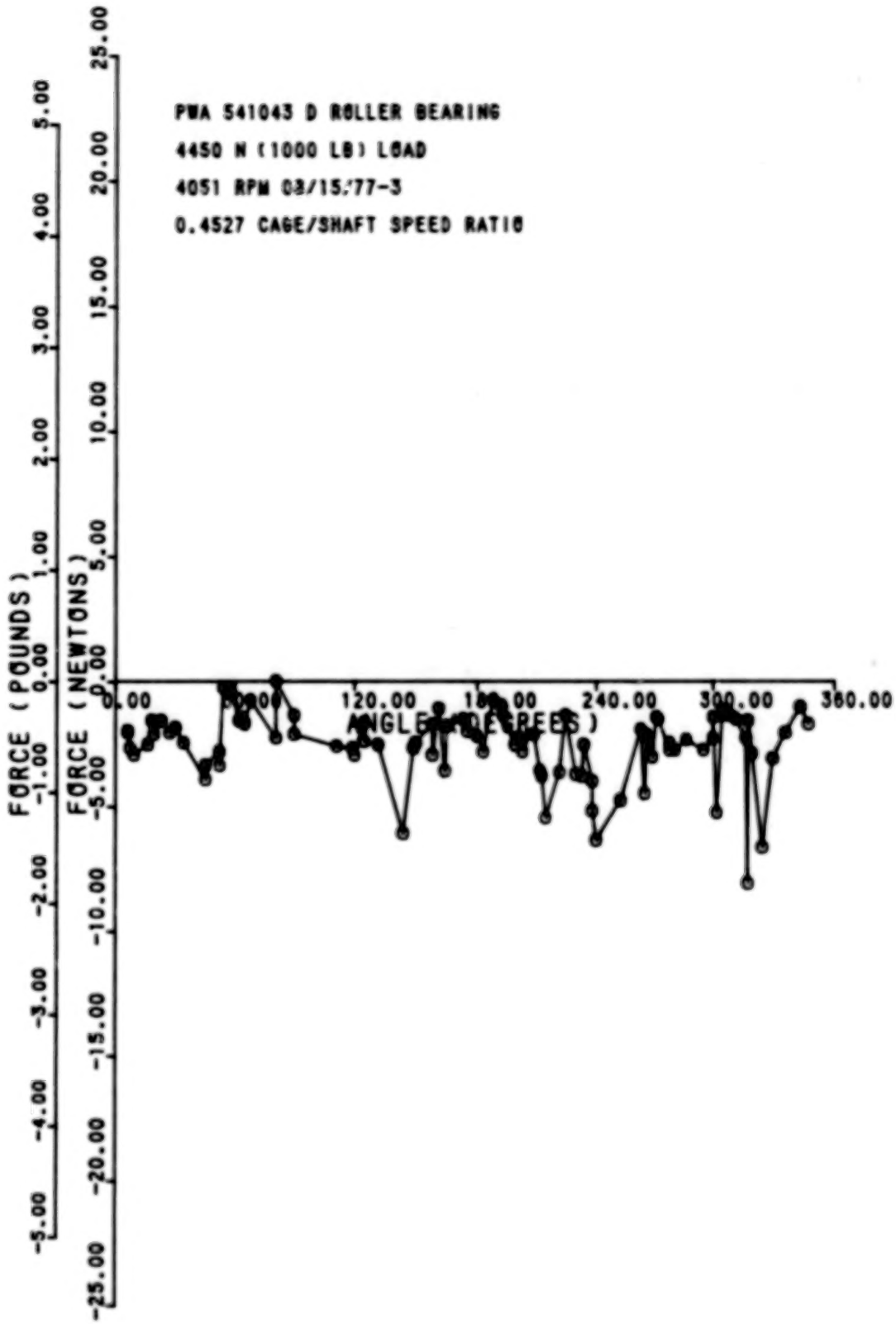

FIG. 3m Roller Contact Forces 0.18 mm Clearance Bearing

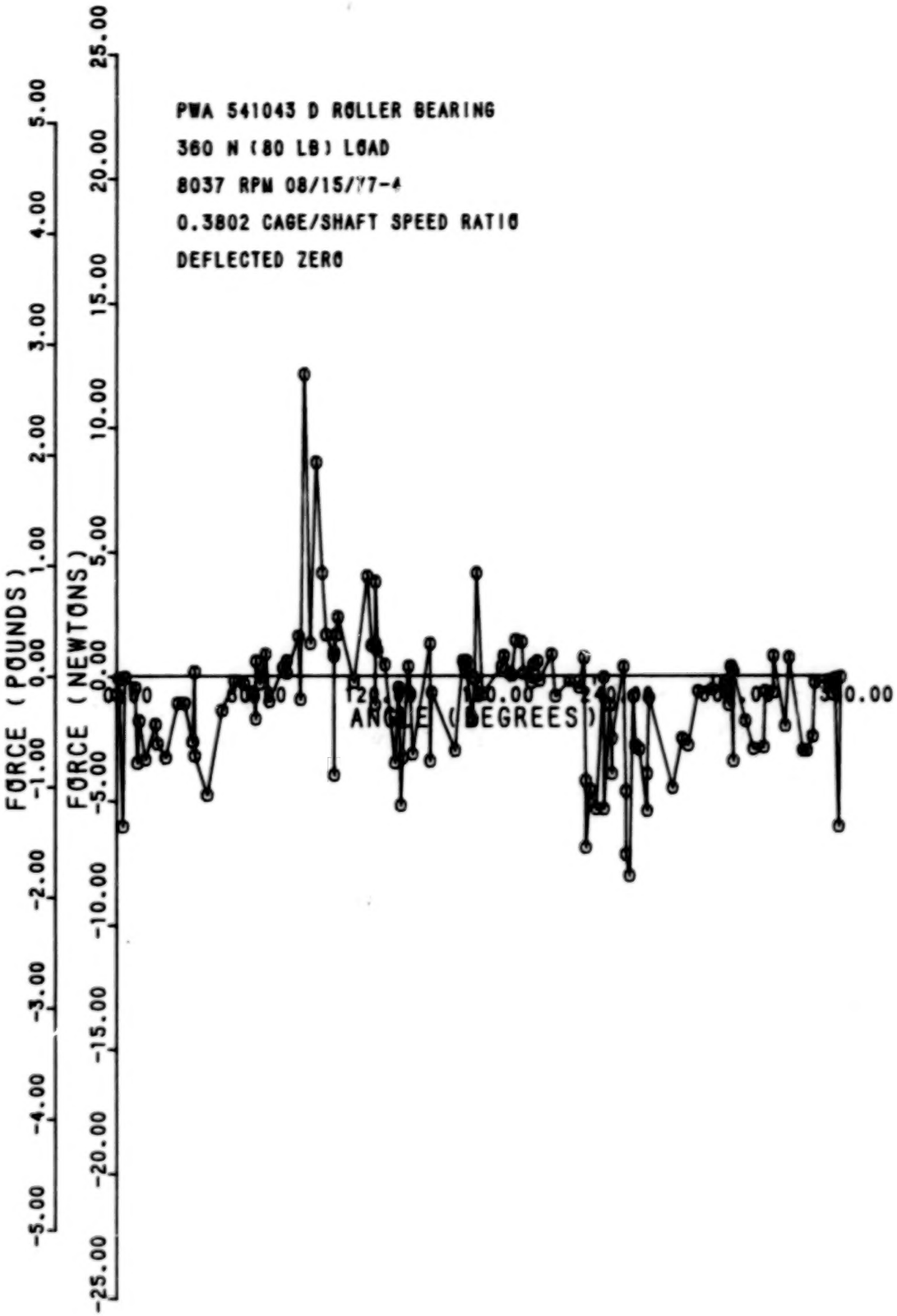

FIG. 3n Roller Contact Forces 0.18 mm Clearance Bearing

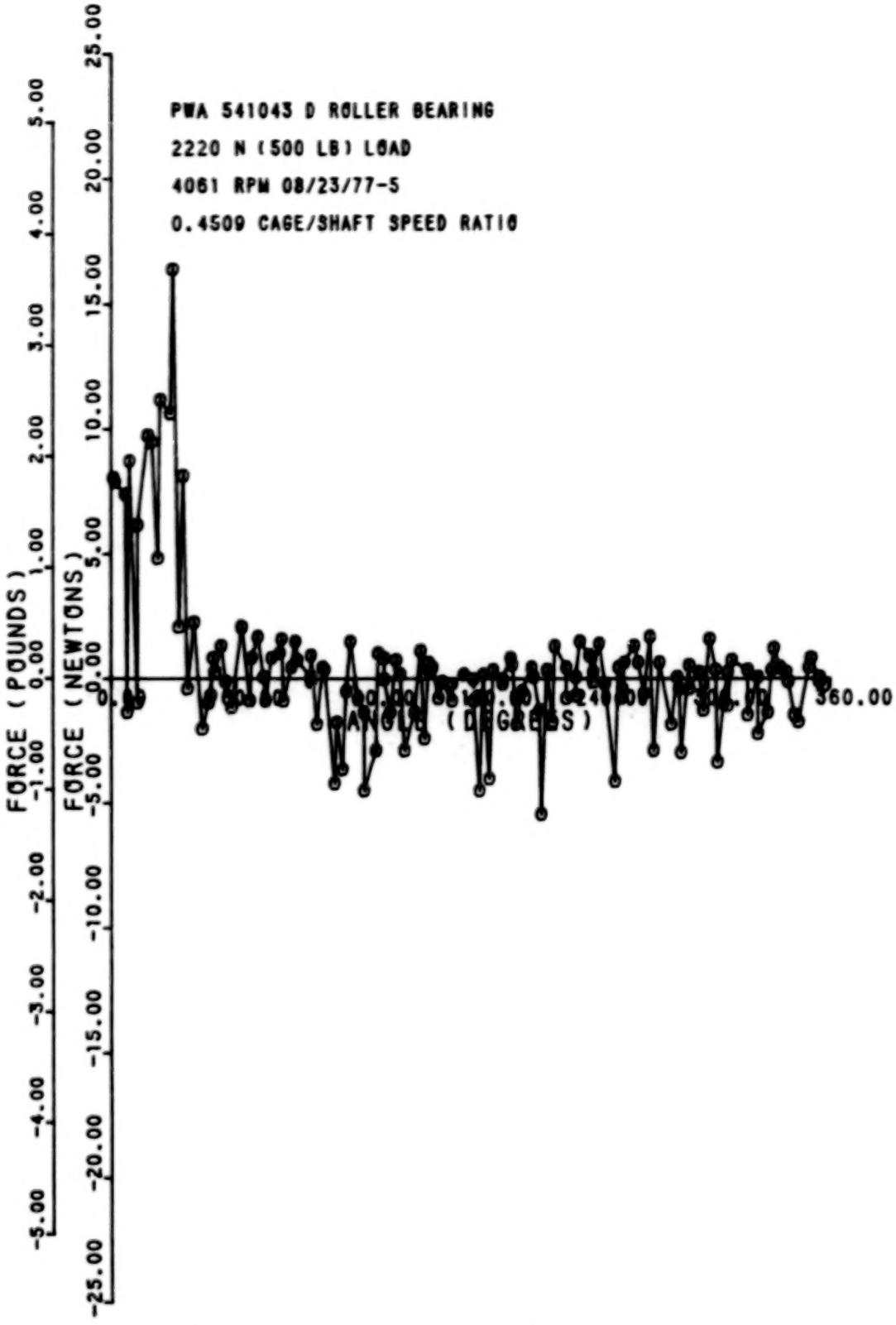

FIG. 3o Roller Contact Forces 0.18 mm Clearance Bearing

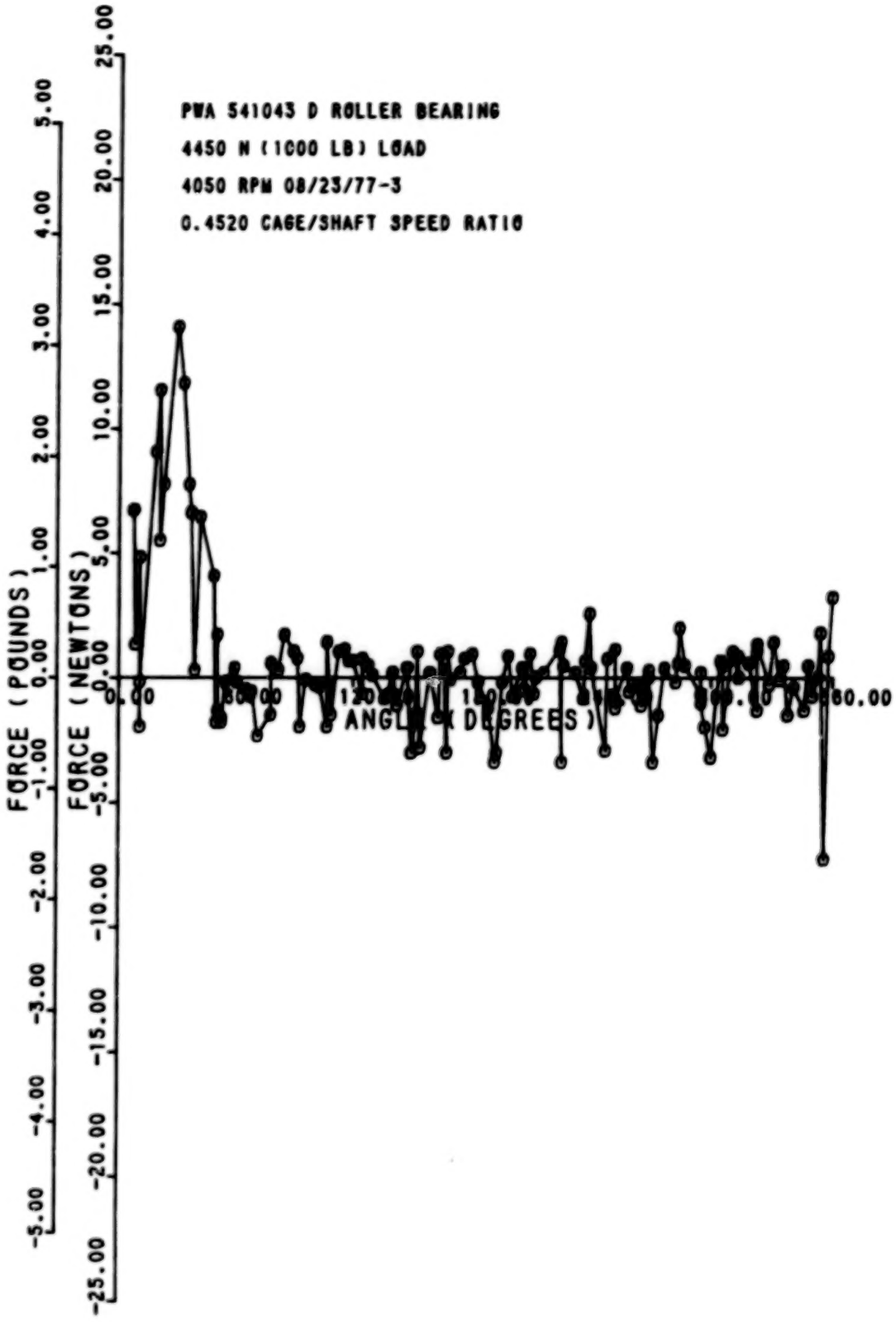

FIG. 3p Roller Contact Forces 0.18 mm Clearance Bearing

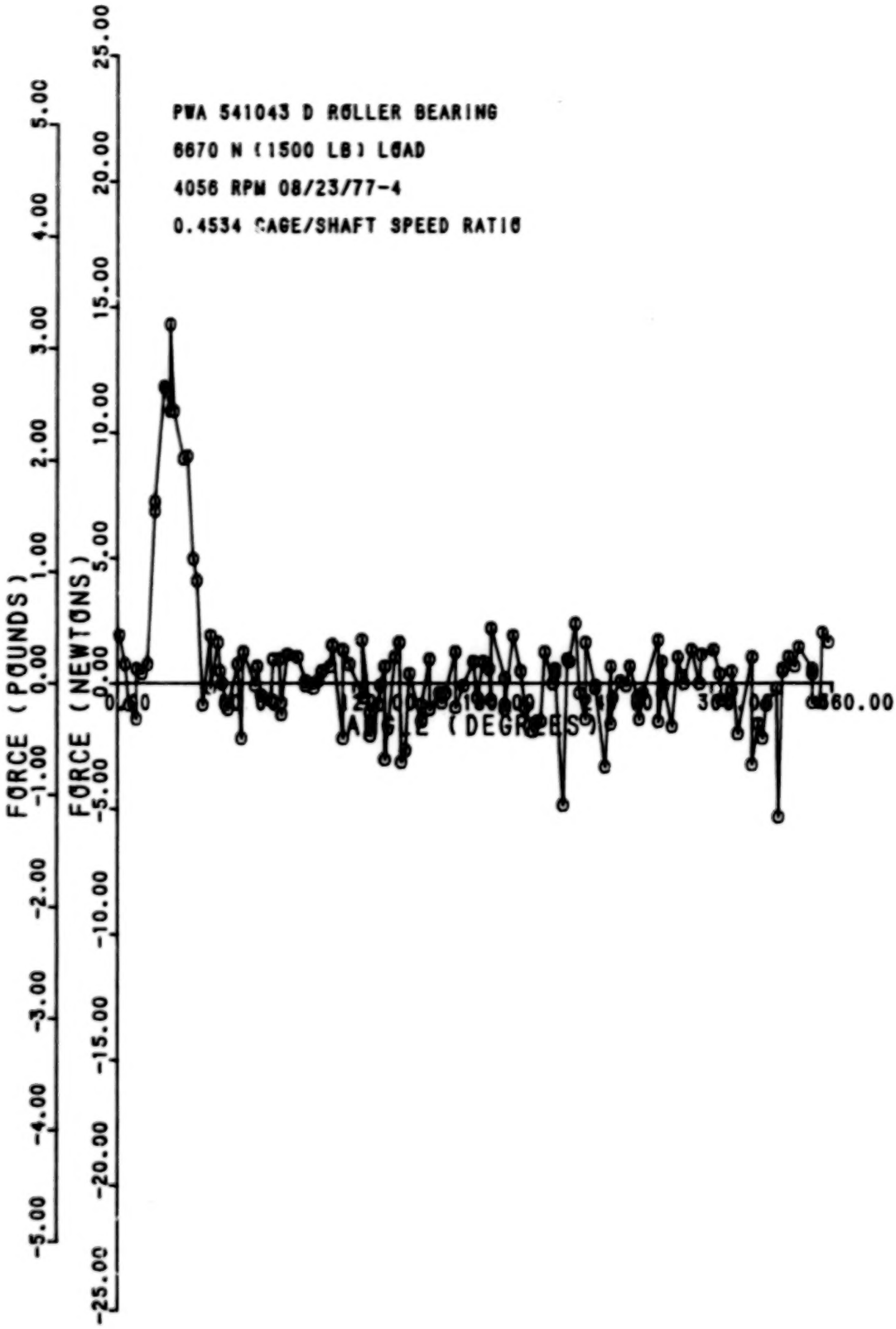

FIG. 3q Roller Contact Forces 0.18 mm Clearance Bearing

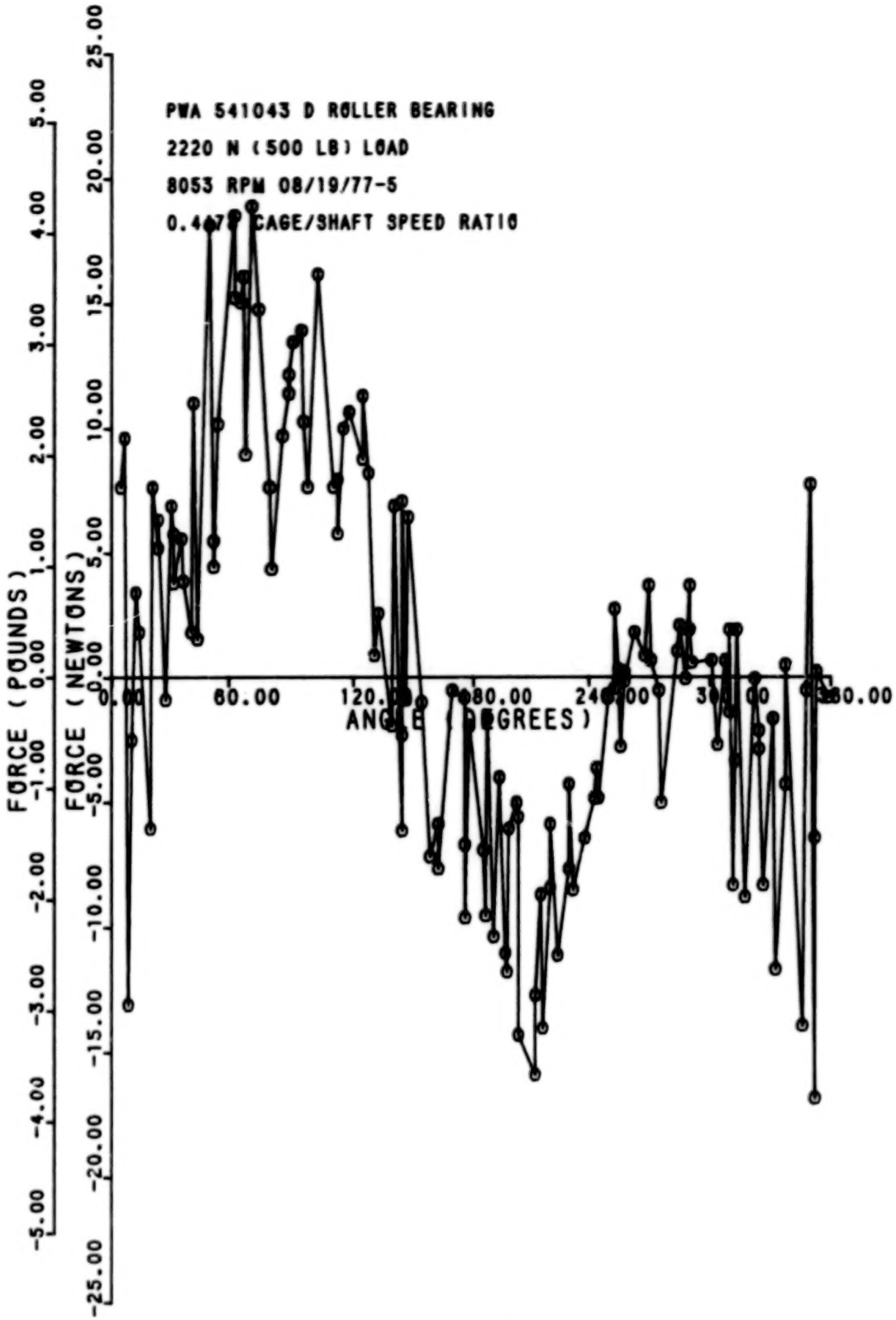

FIG. 3r Roller Contact Forces 0.18 mm Clearance Bearing

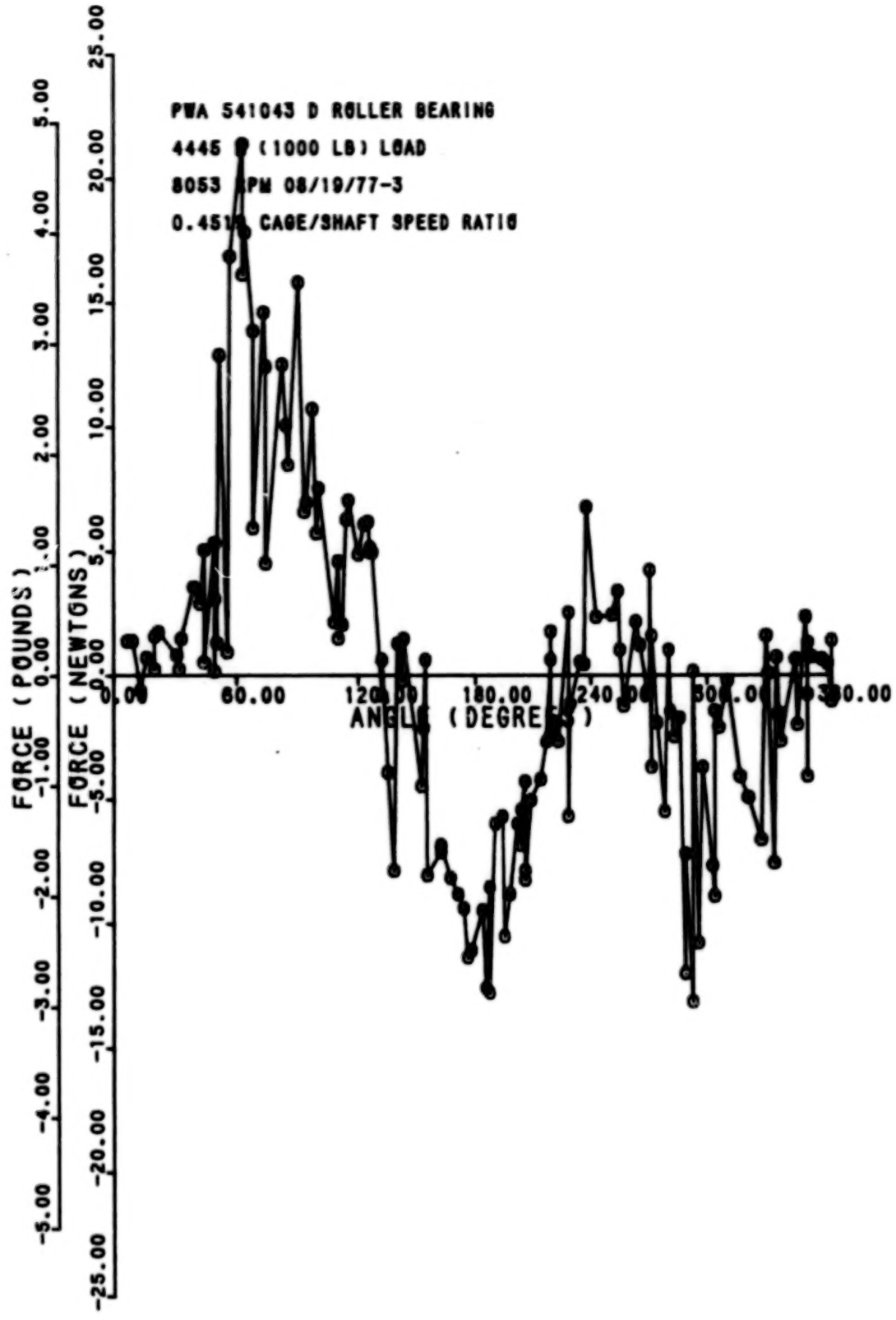

FIG. 3s Roller Contact Forces 0.18 mm Clearance Bearing

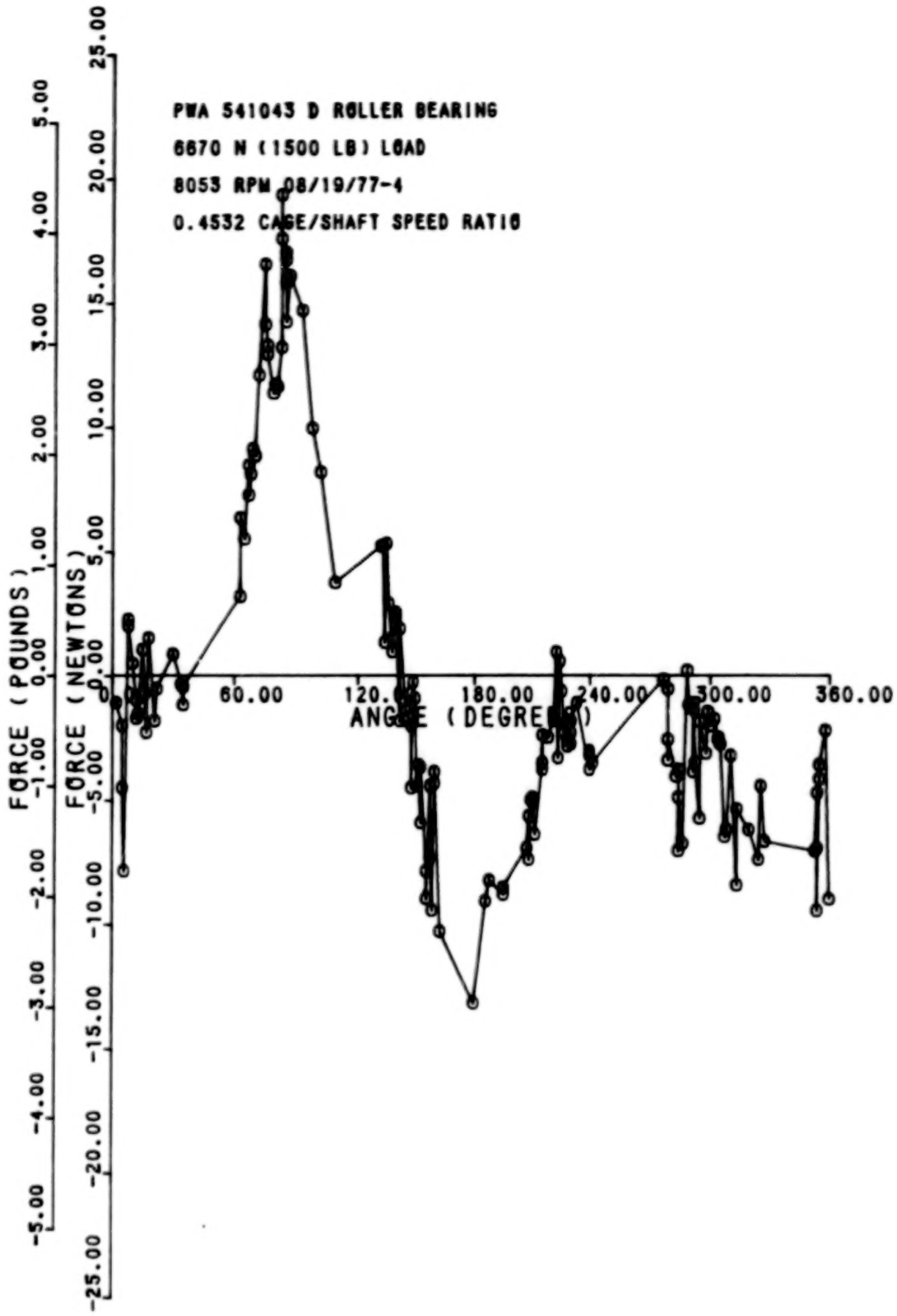

FIG. 3t Roller Contact Forces 0.18 mm Clearance Bearing

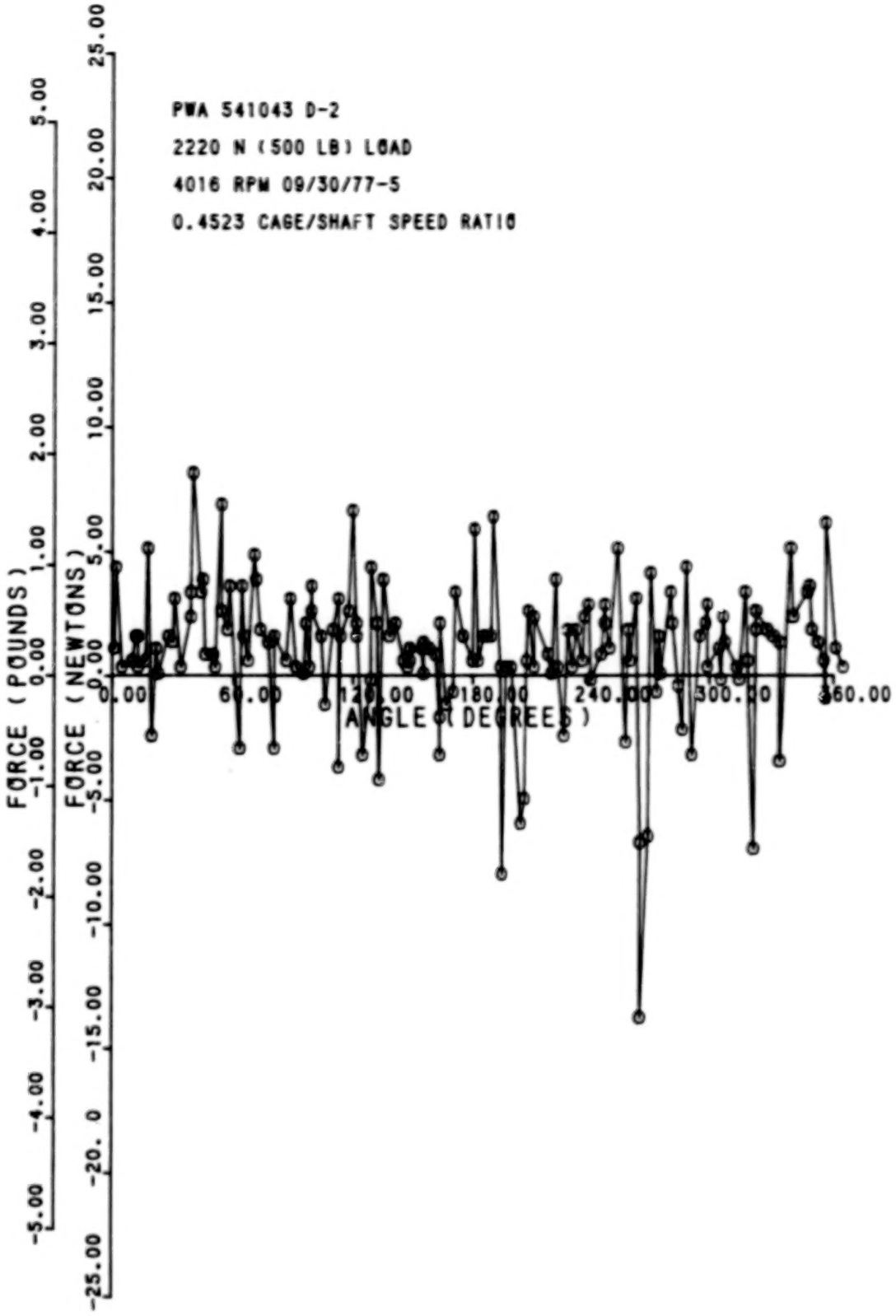

FIG. 4a Roller Contact Forces 0.21 mm Clearance Bearing

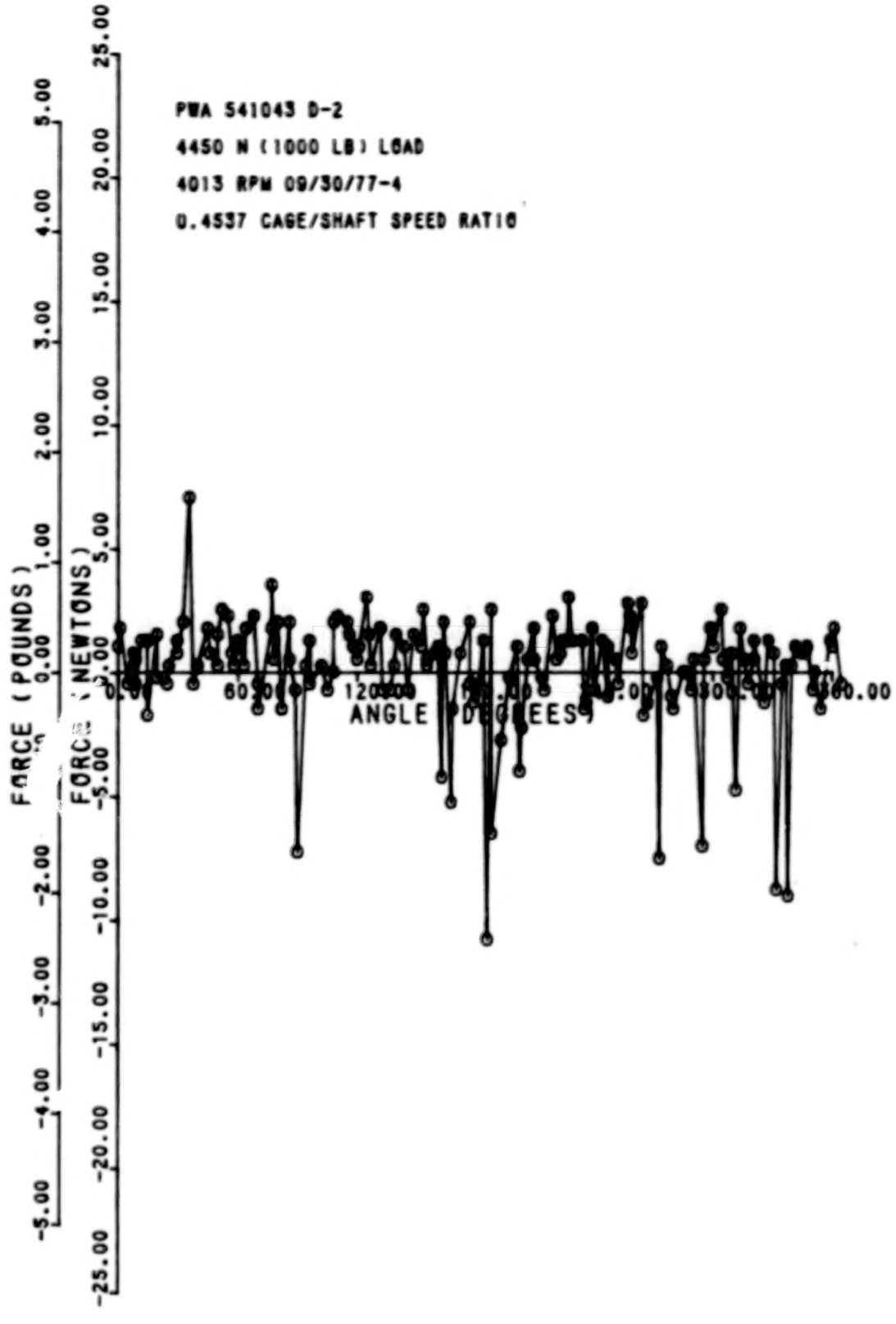

FIG. 4b Roller Contact Forces 0.21 mm Clearance Bearing

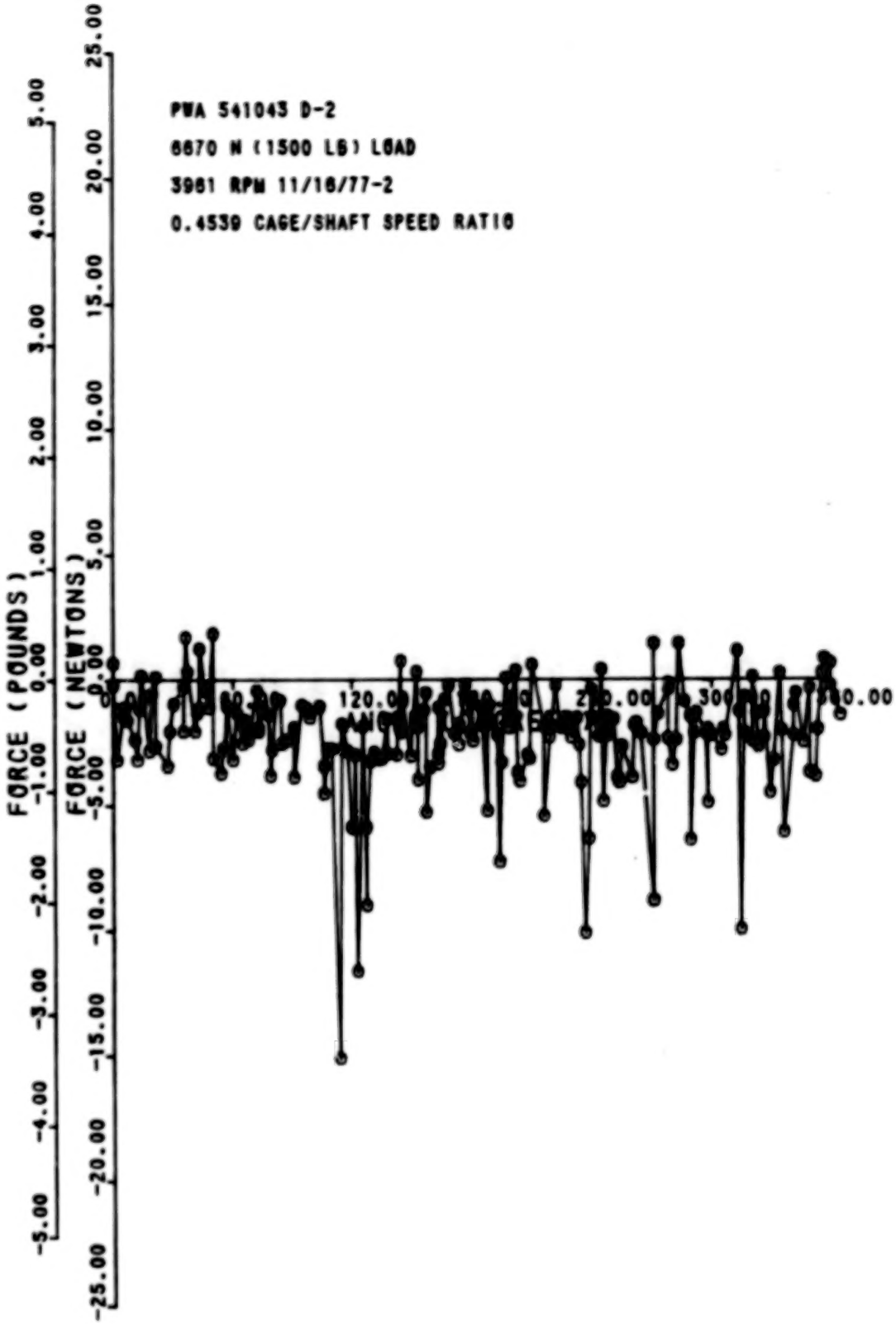

FIG. 4c Roller Contact Forces 0.21 mm Clearance Bearing

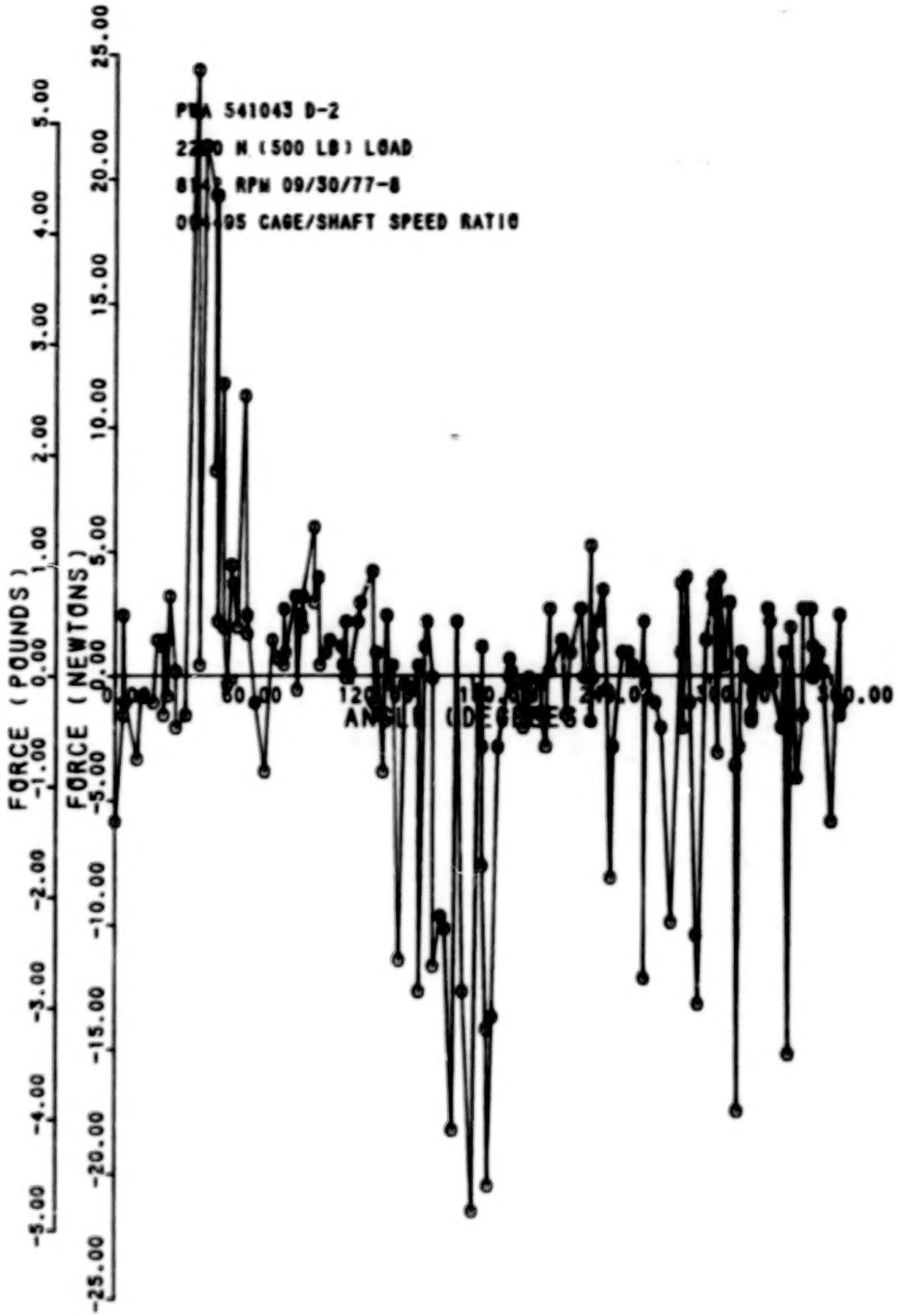

FIG. 4d Roller Contact Forces 0.21 mm Clearance Bearing

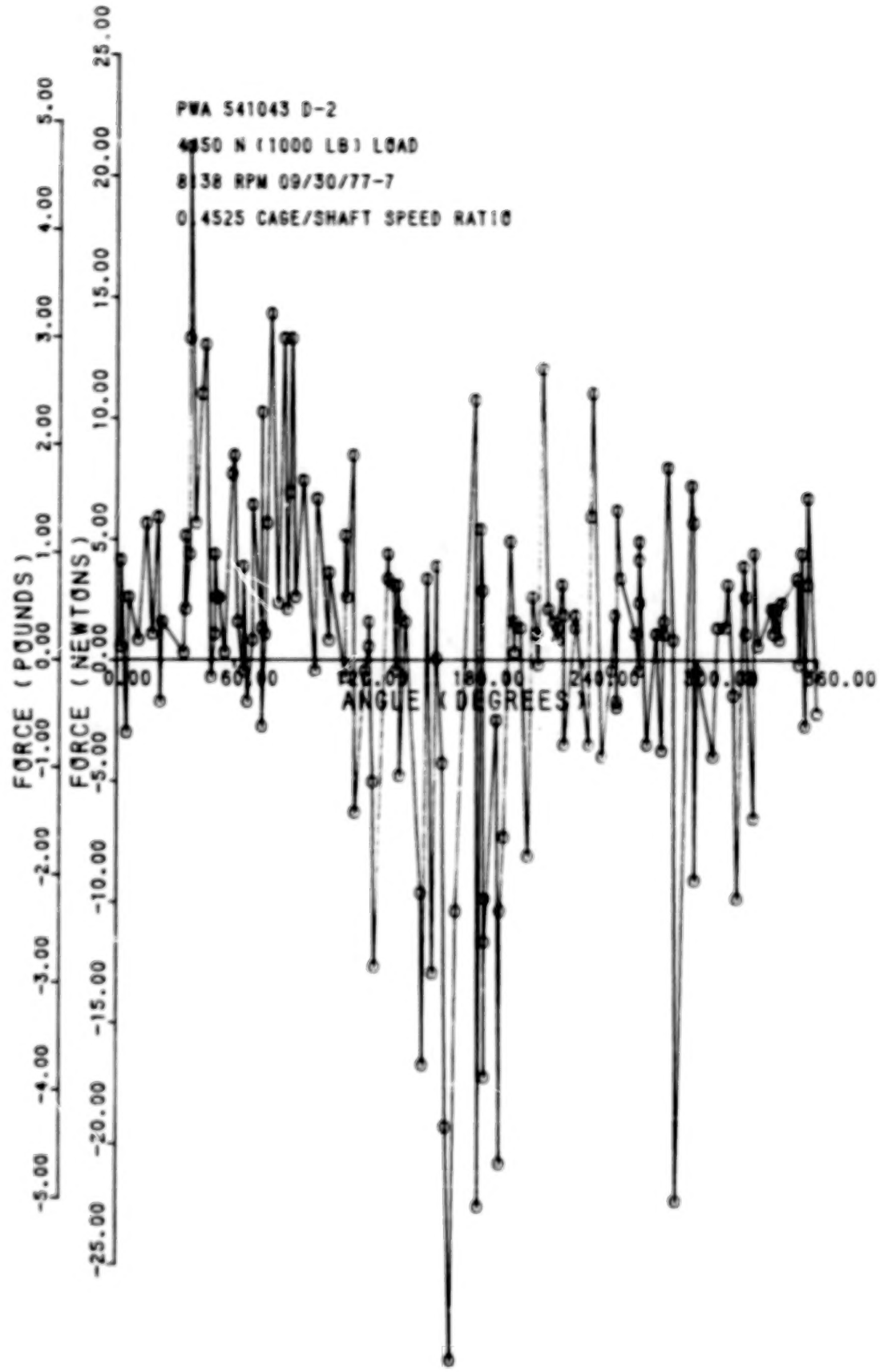

FIG. 4e Roller Contact Forces 0.21 mm Clearance Bearing

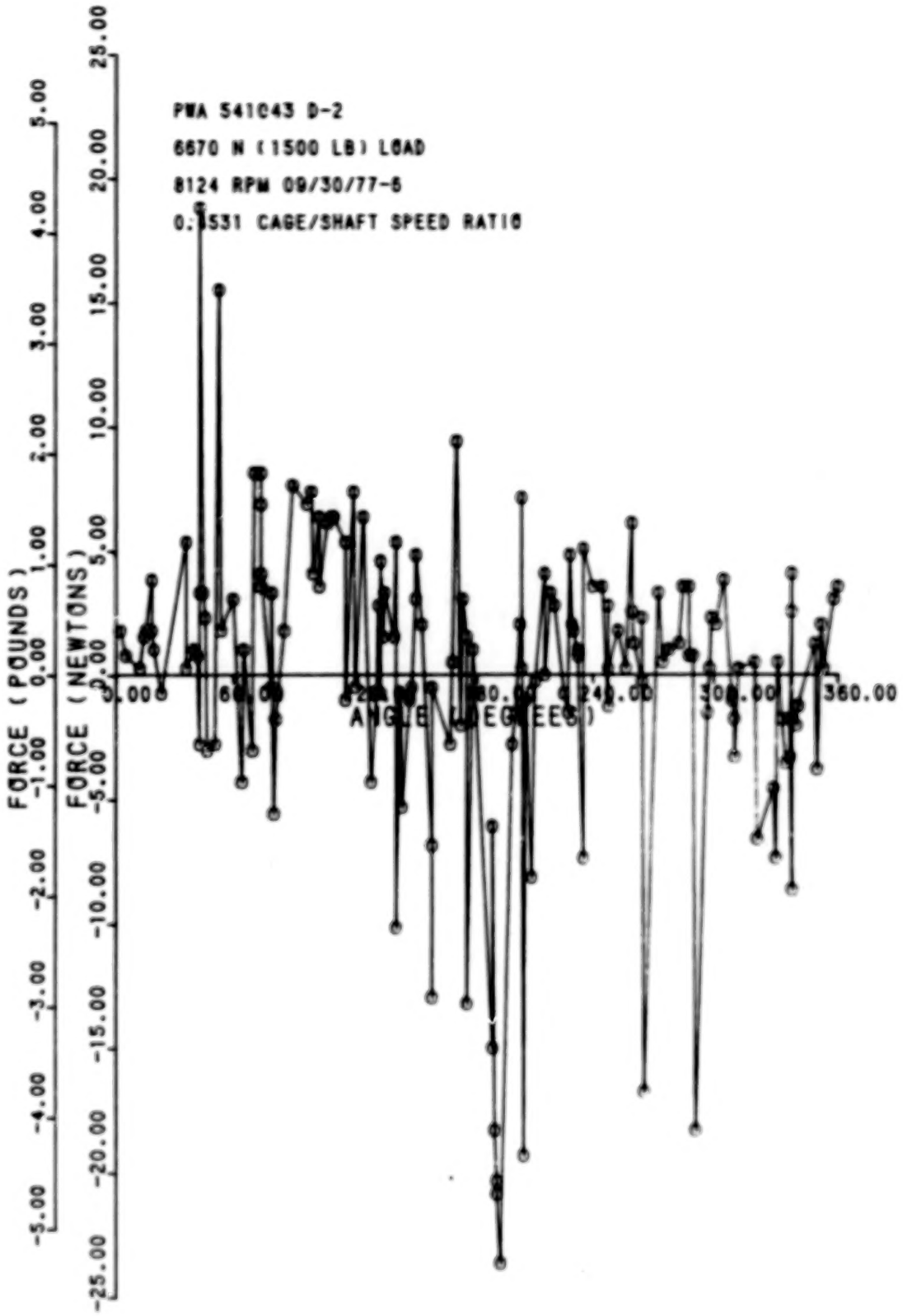

FIG. 4f [illegible]ller Contact Forces 0.21 mm Clearance Bearing

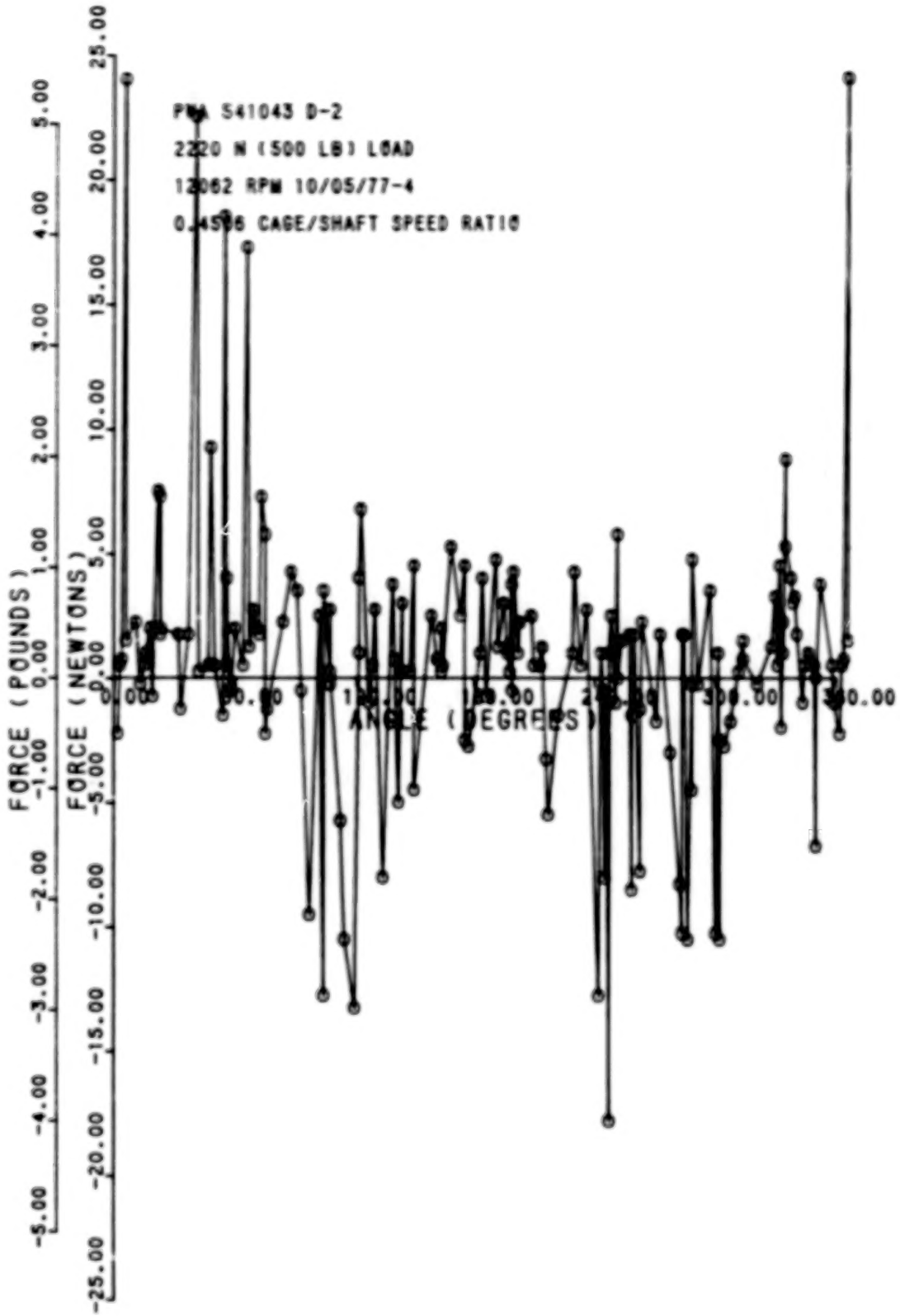

FIG. 4g Roller Contact Forces 0.21 mm Clearance Bearing

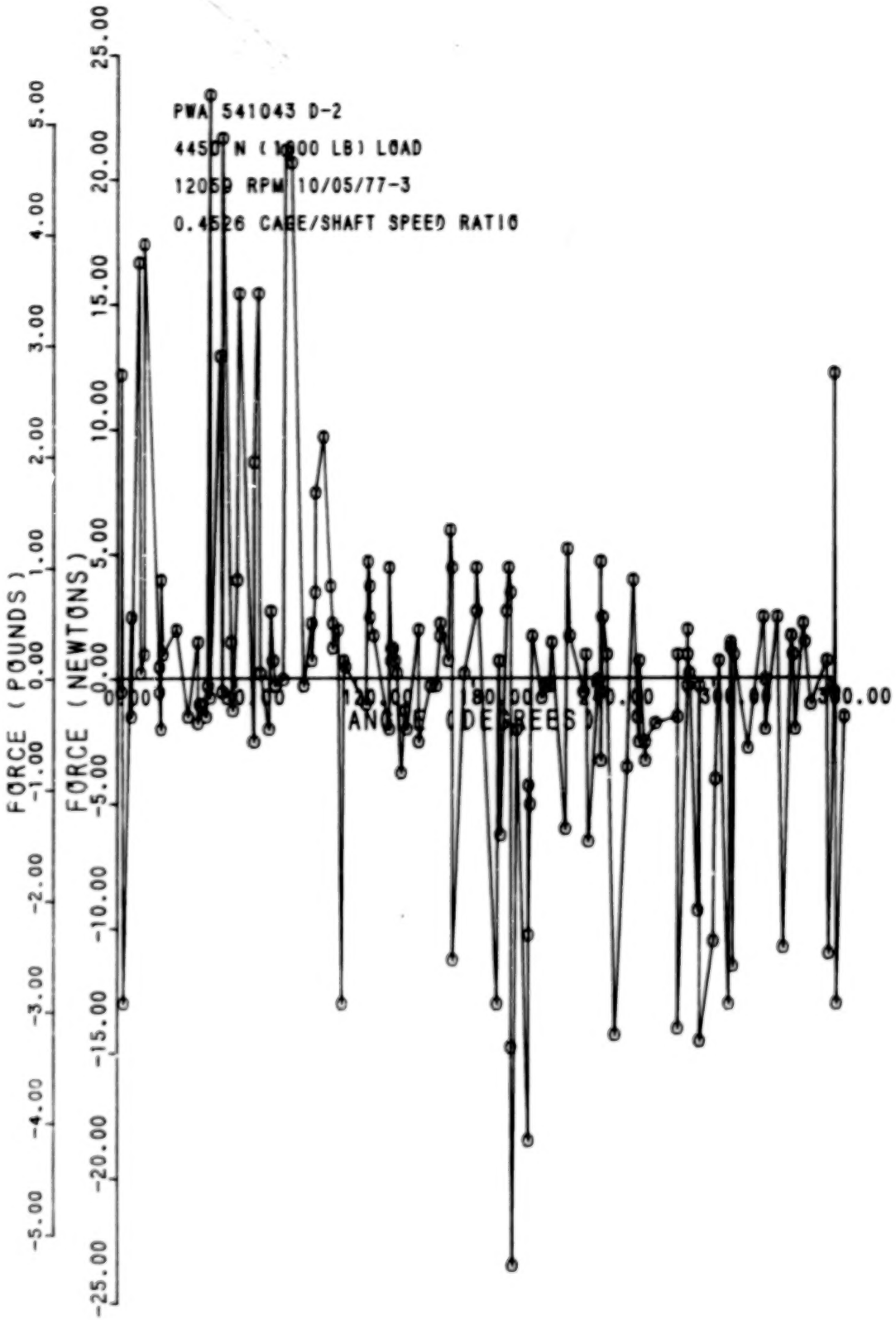

FIG. 4h Roller Contact Forces 0.21 mm Clearance Bearing

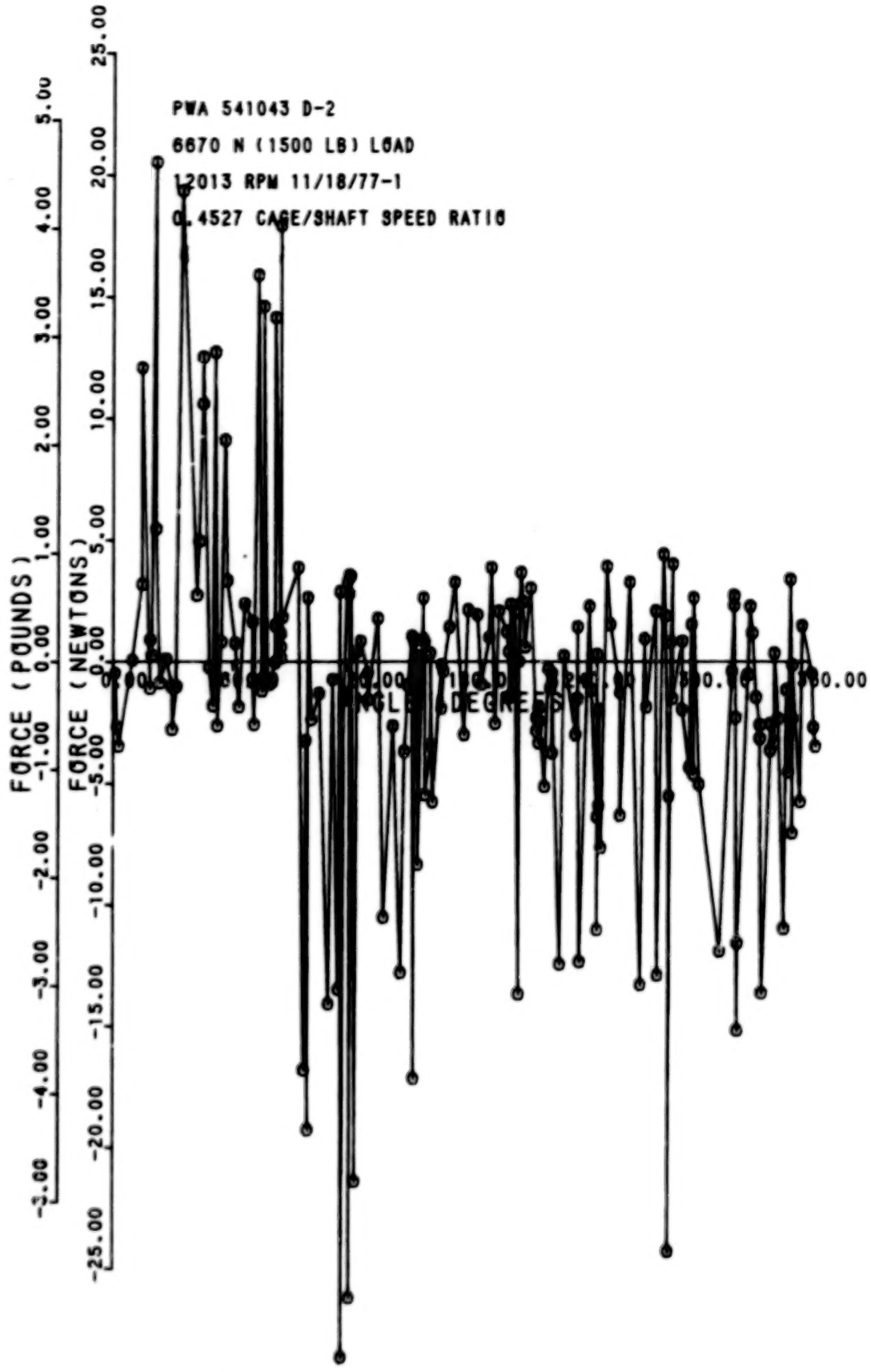

FIG. 41 Roller Contact Forces 0.21 mm [illegible]earance Bearing

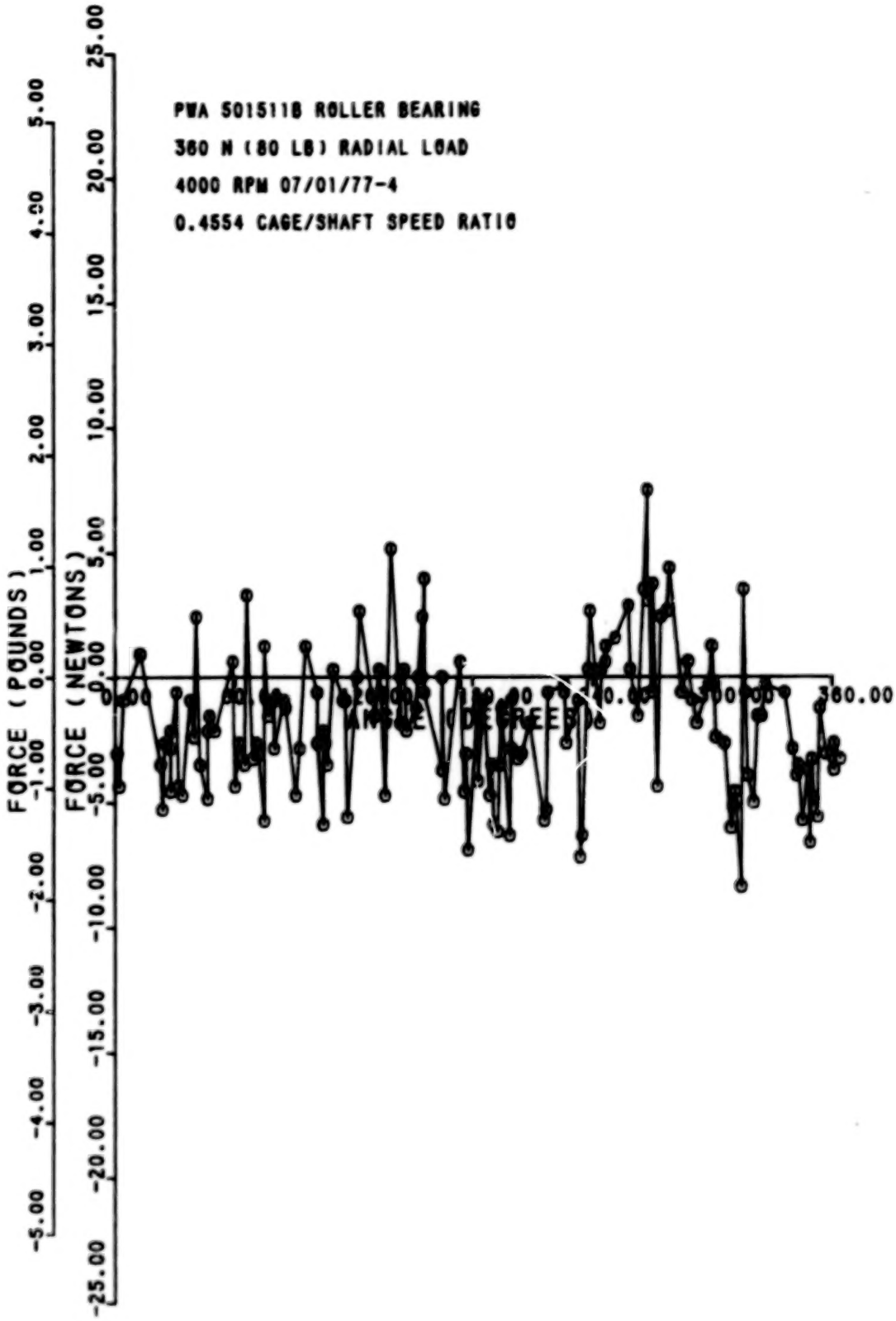

FIG. 5a Roller Contact Forces Out-of-Round Outer Raceway Bearing

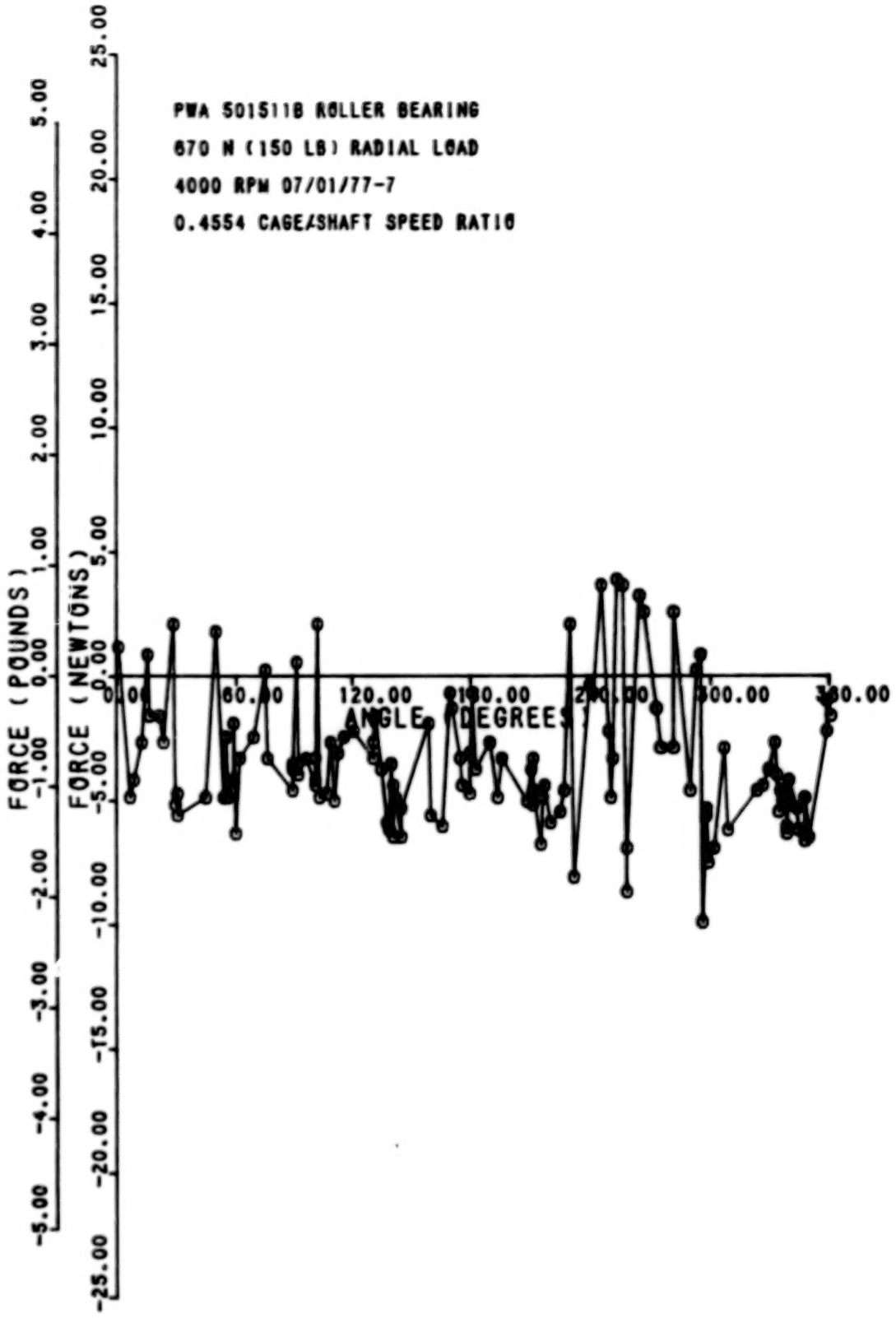

FIG. 5b Roller Contact Forces Out-of-Round Outer Raceway Bearing

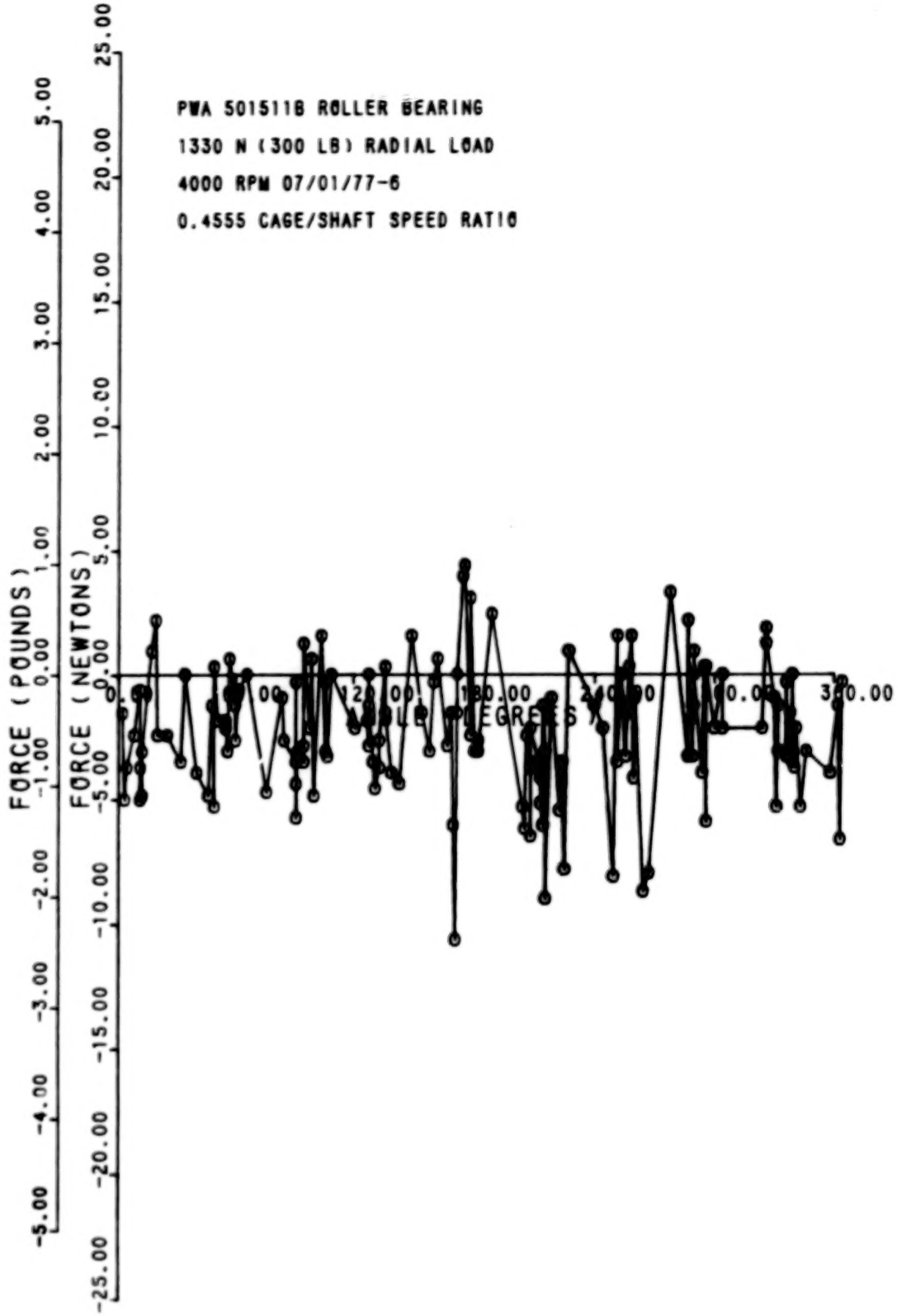

FIG. 5c Roller Contact Forces Out-of-Round Outer Raceway Bearing

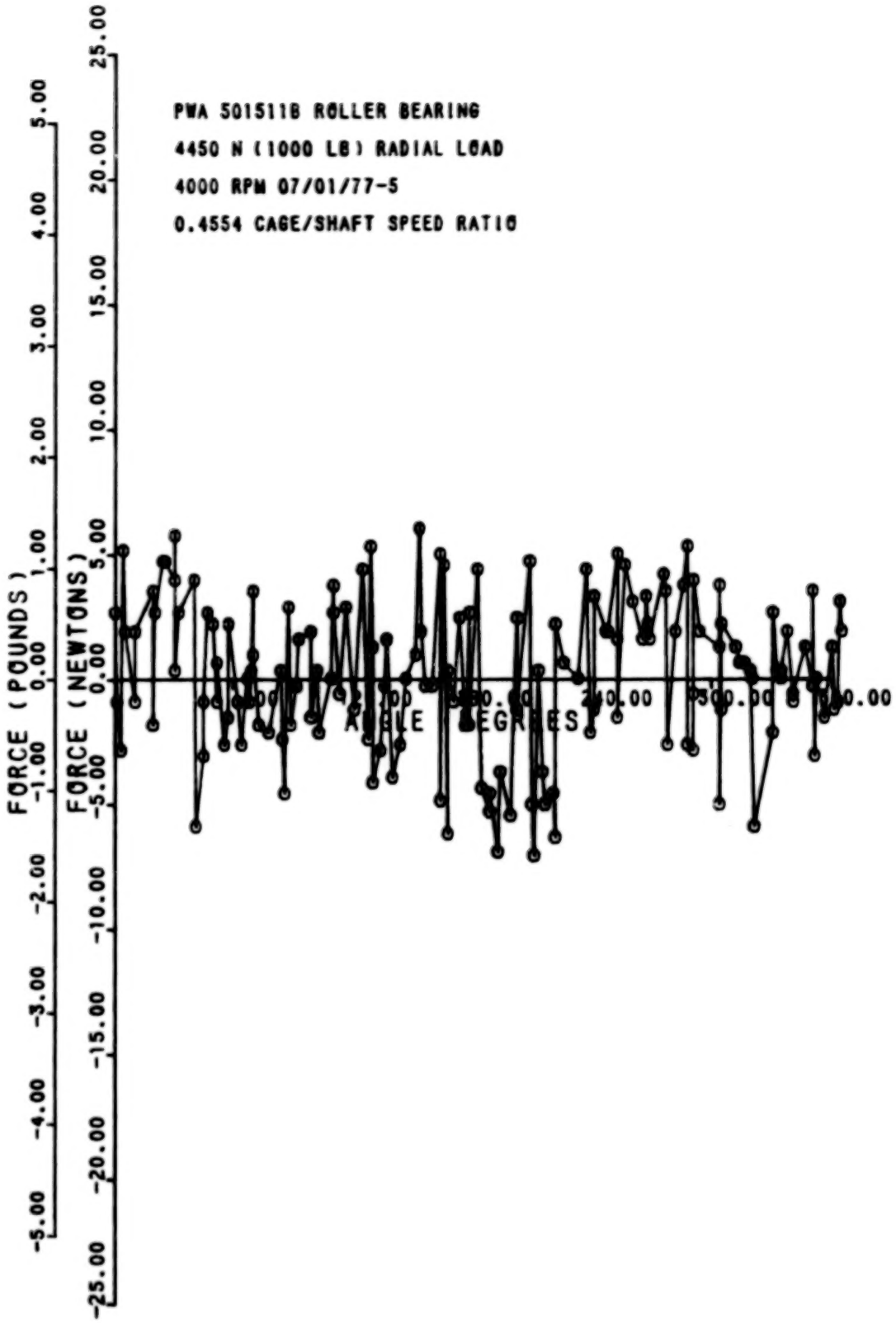

FIG. 5d Roller Contact Forces Out-of-Round Outer Raceway Bearing

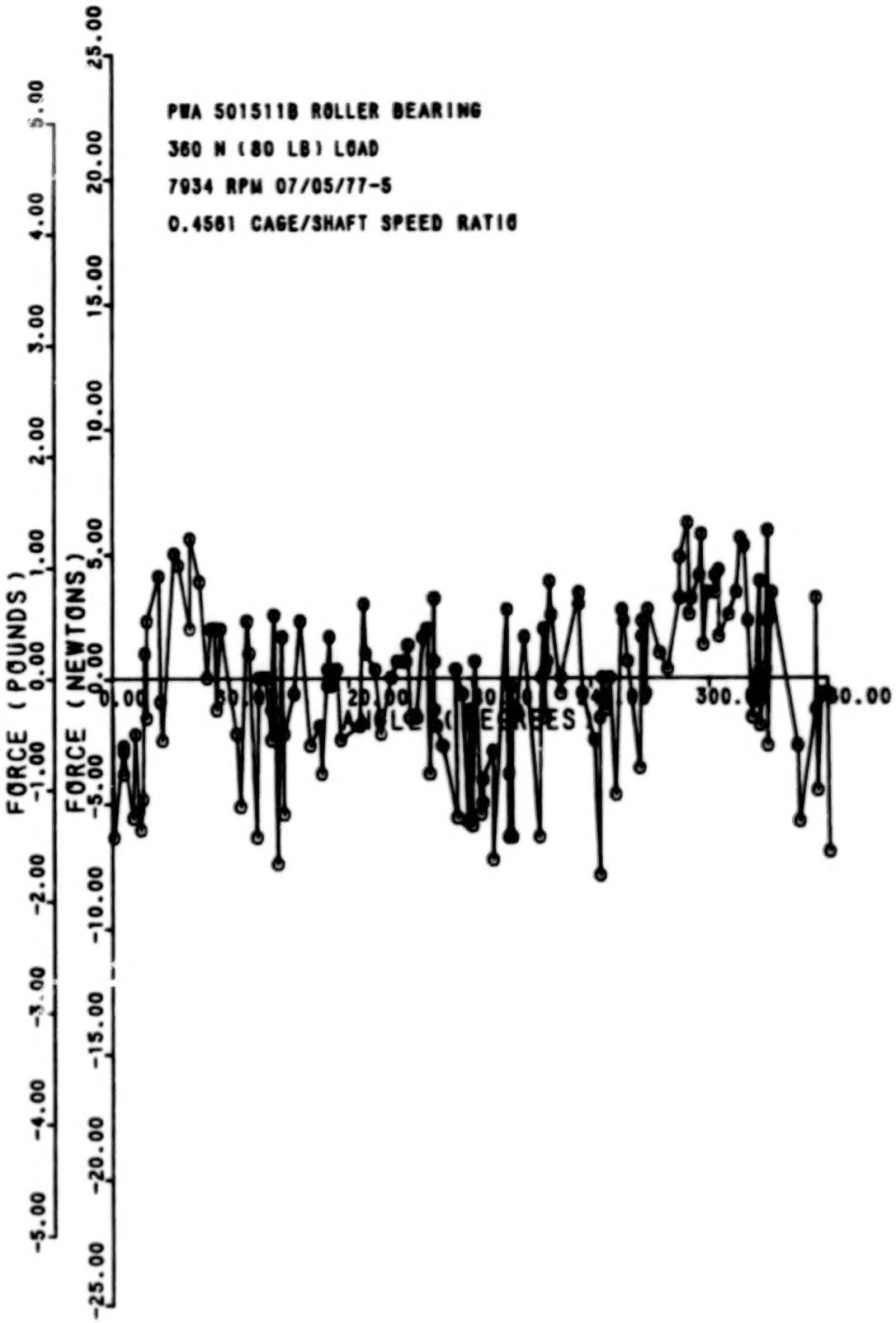

FIG. 5e Roller Contact Forces Out-of-Round Outer Raceway Bearing

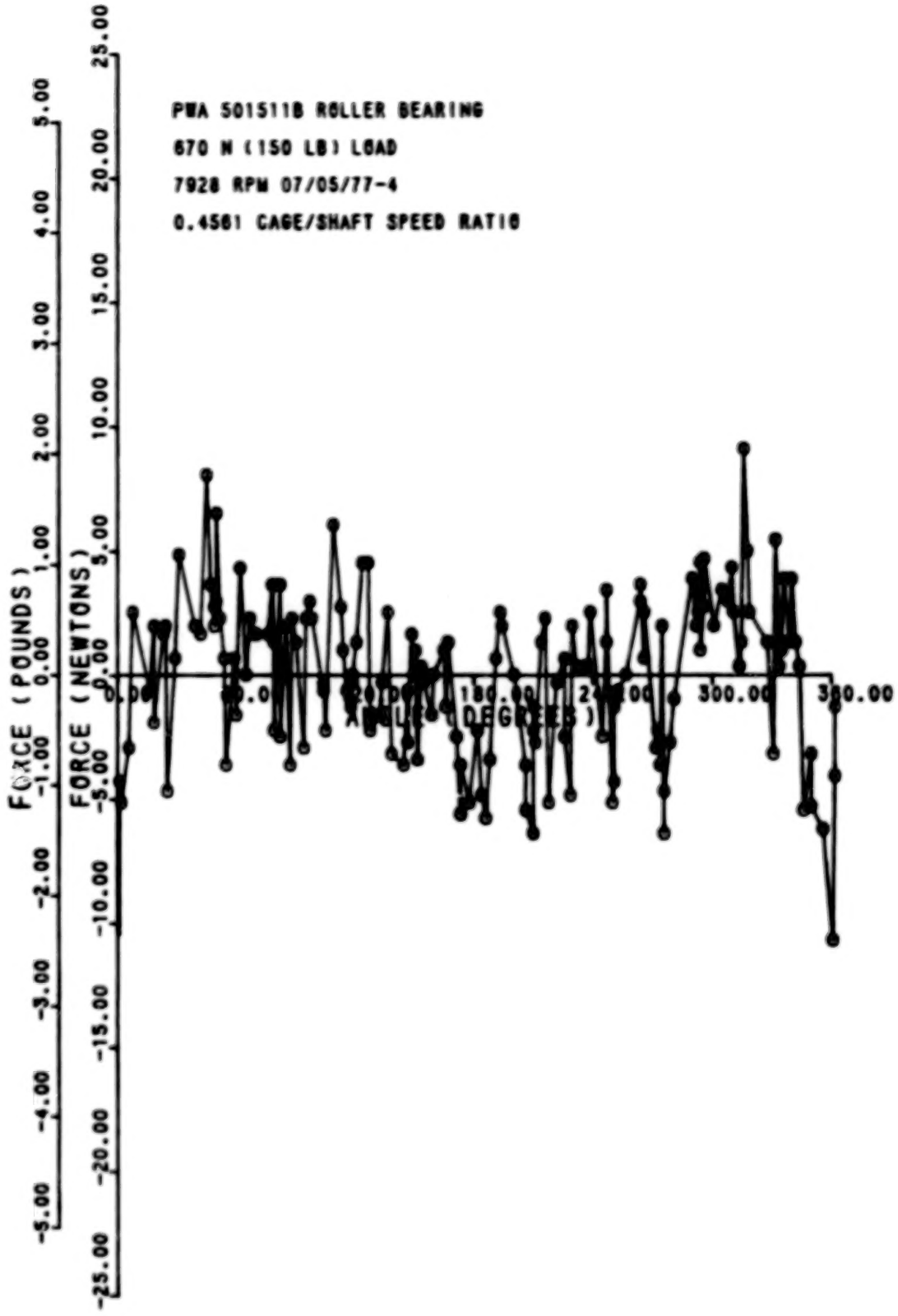

FIG. 5f Roller Contact Forces Out-of-Round Outer Raceway Bearing

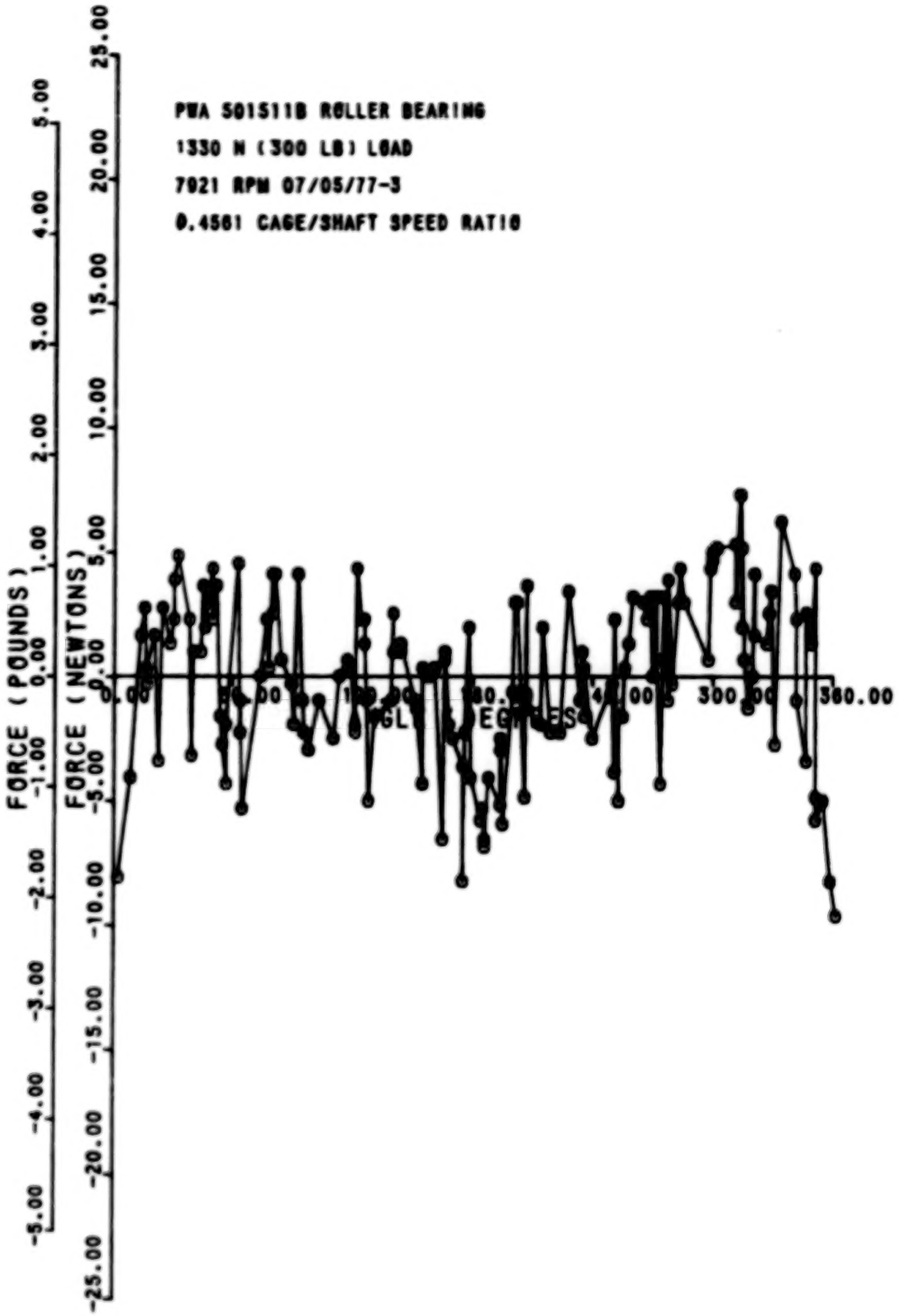

FIG. 5g Roller Contact Forces Out-of-Round Outer Raceway Bearing

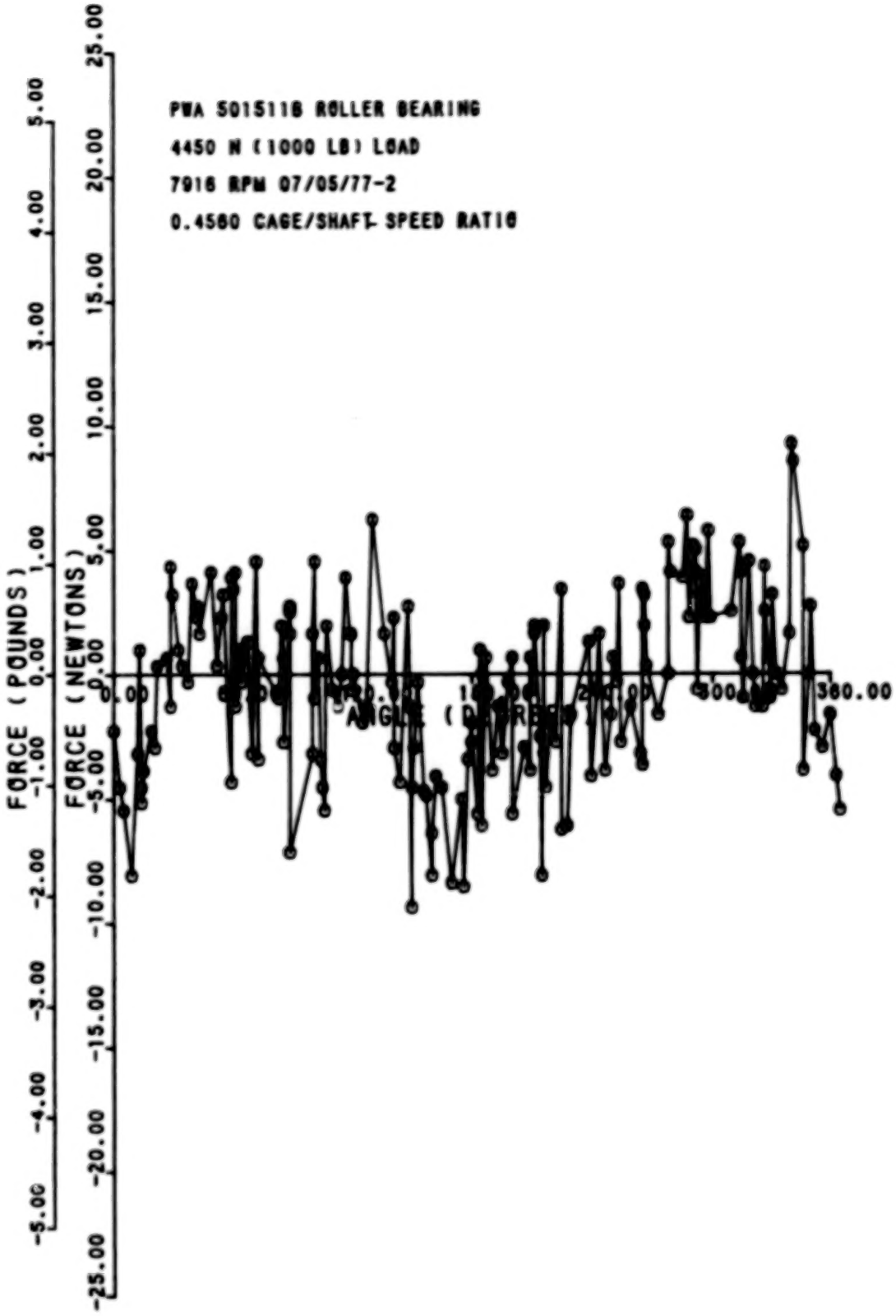

FIG. 5h Roller Contact Forces Out-of-Round Outer Raceway Bearing

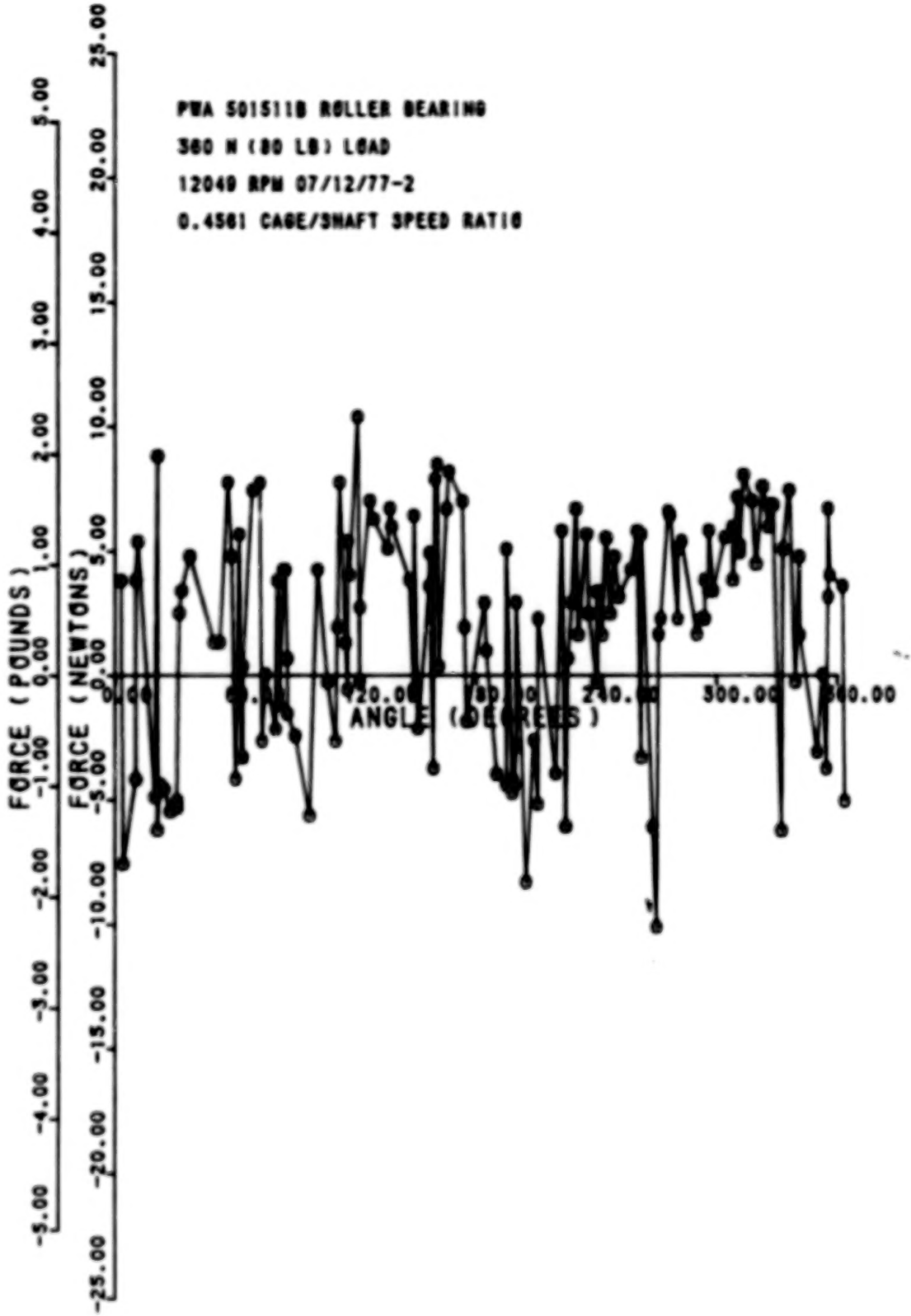

FIG. 5i Roller Contact Forces Out-of-Round Outer Raceway Bearing

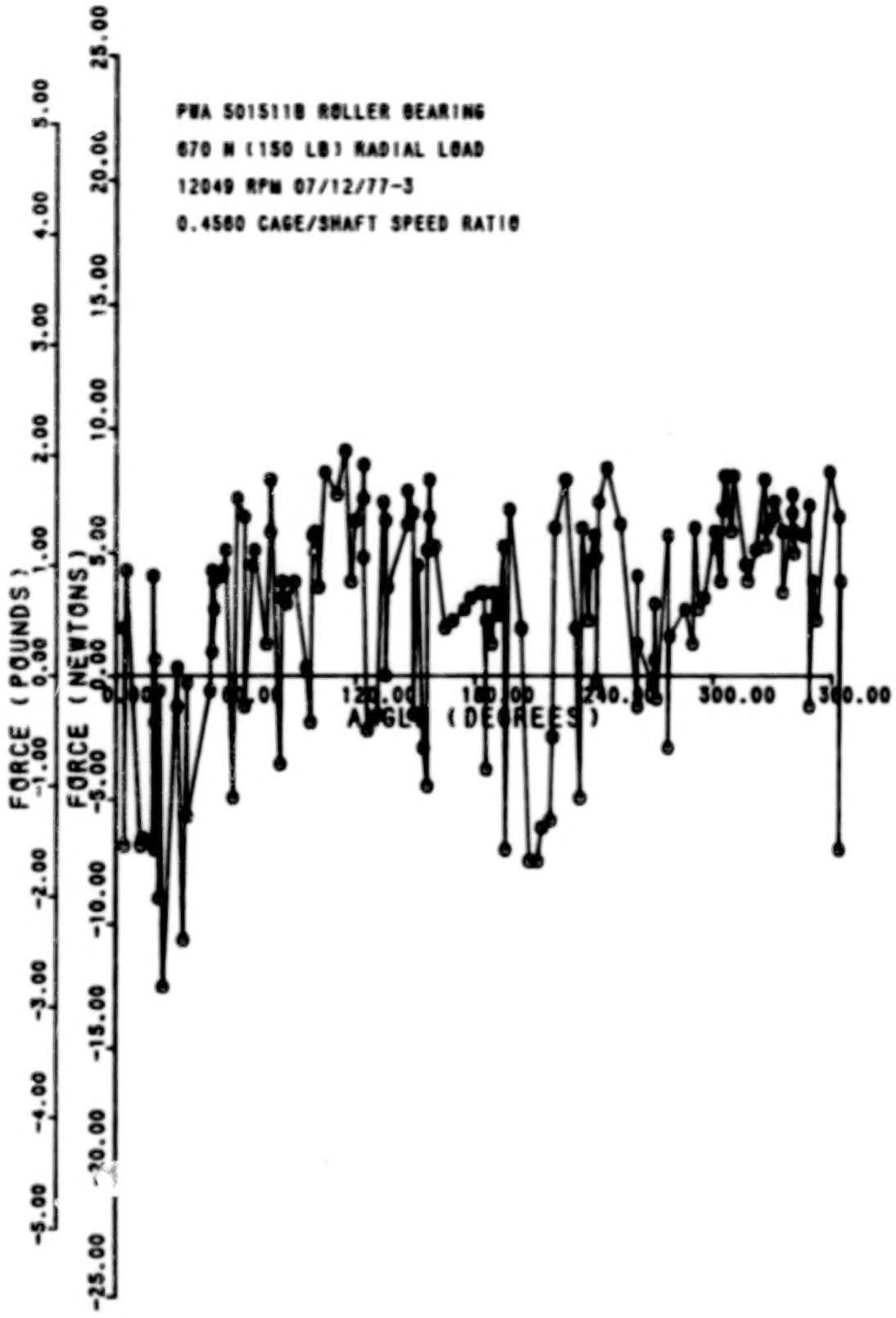

FIG. 5j Roller Contact Forces Out-of-Round Outer Raceway Bearing

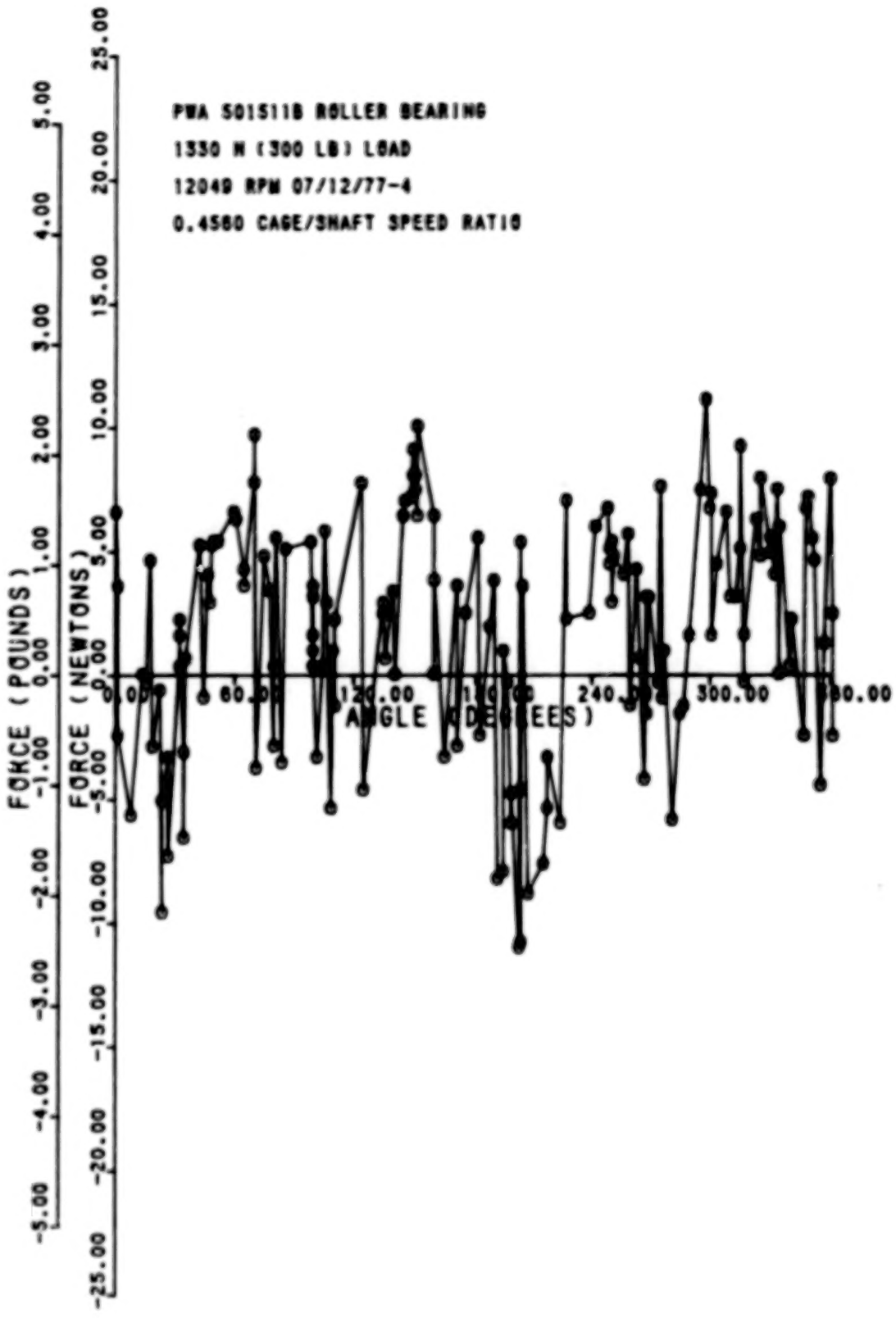

FIG. 5k Roller Contact Forces Out-of-Round Outer Raceway Bearing

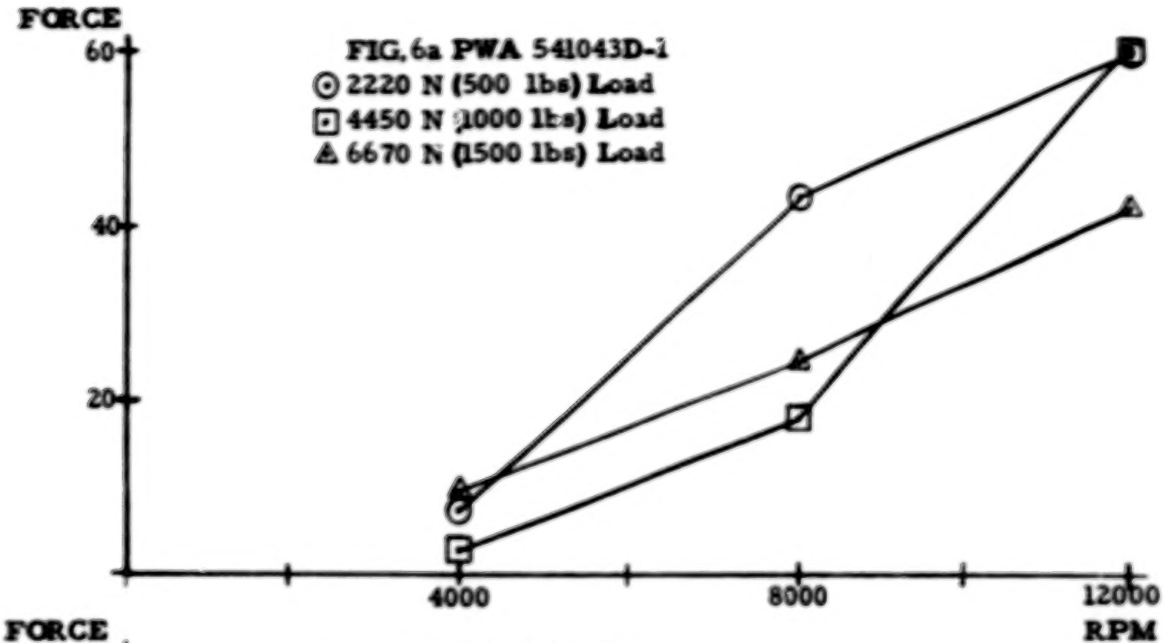

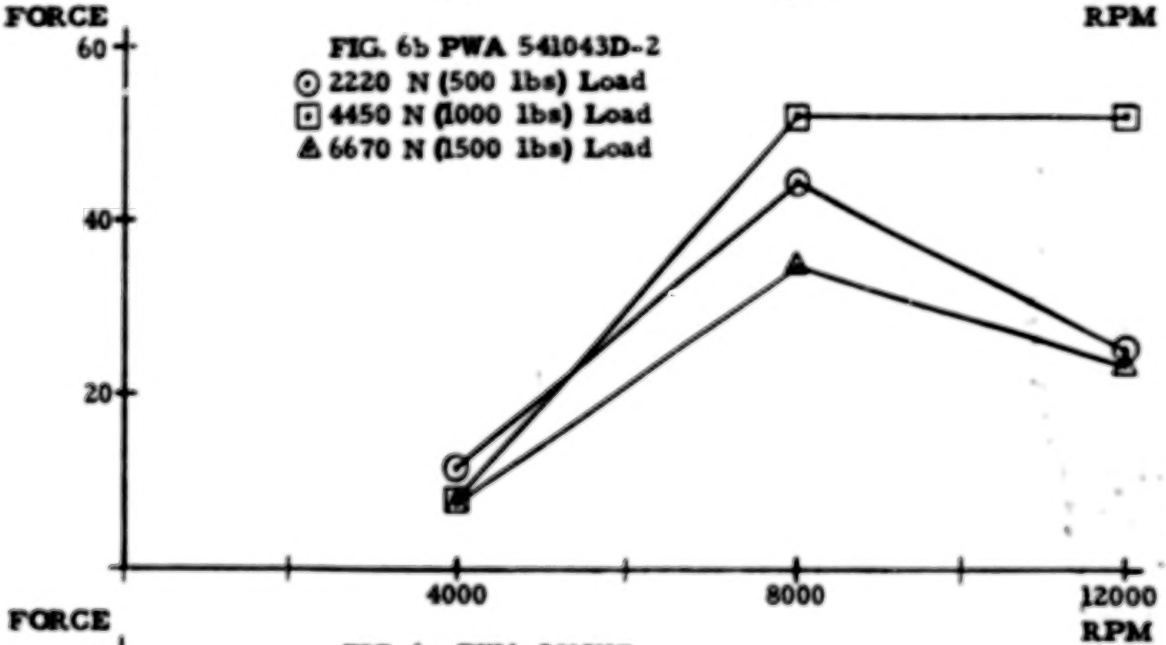

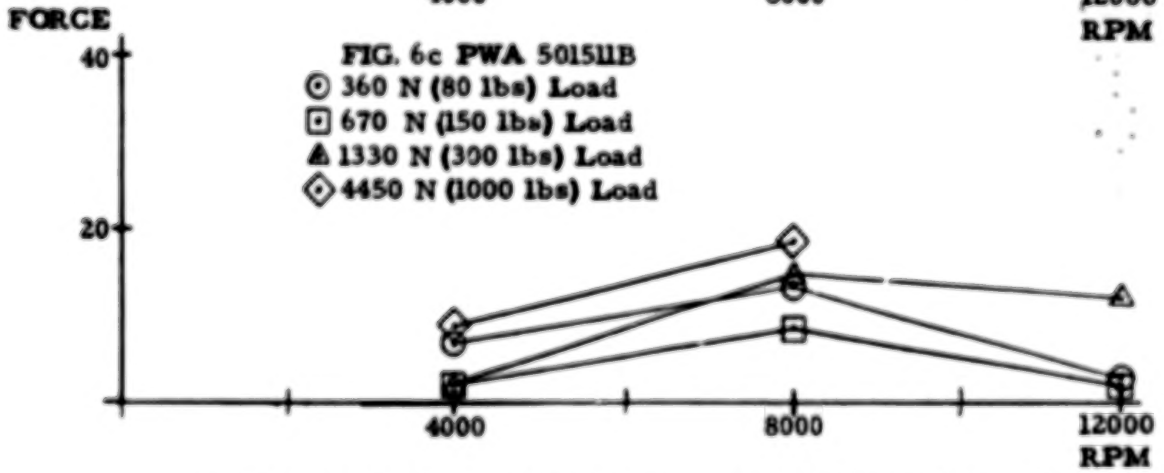

FIGS. 6a-c Resultant Cage Force Magnitude Versus Shaft Speed

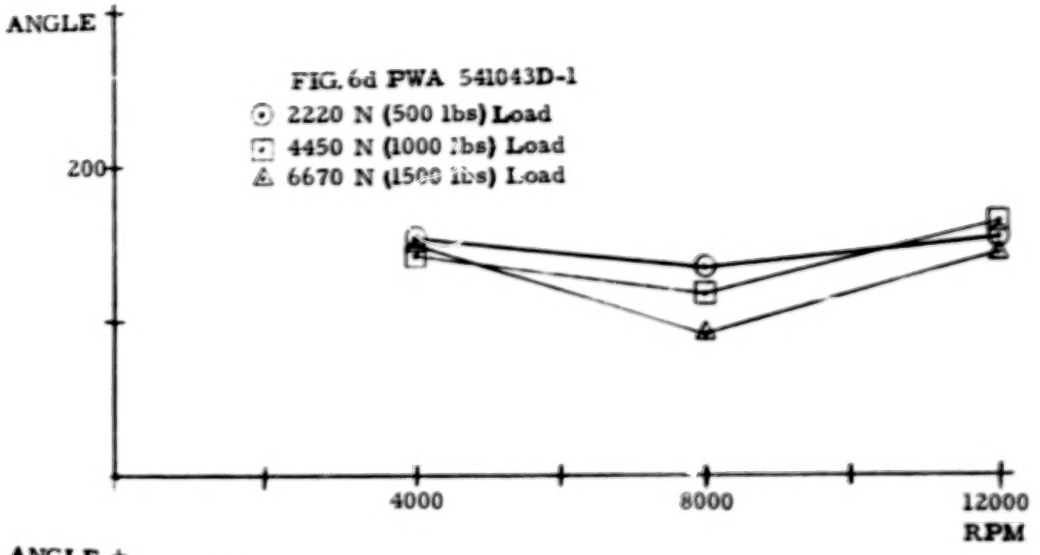

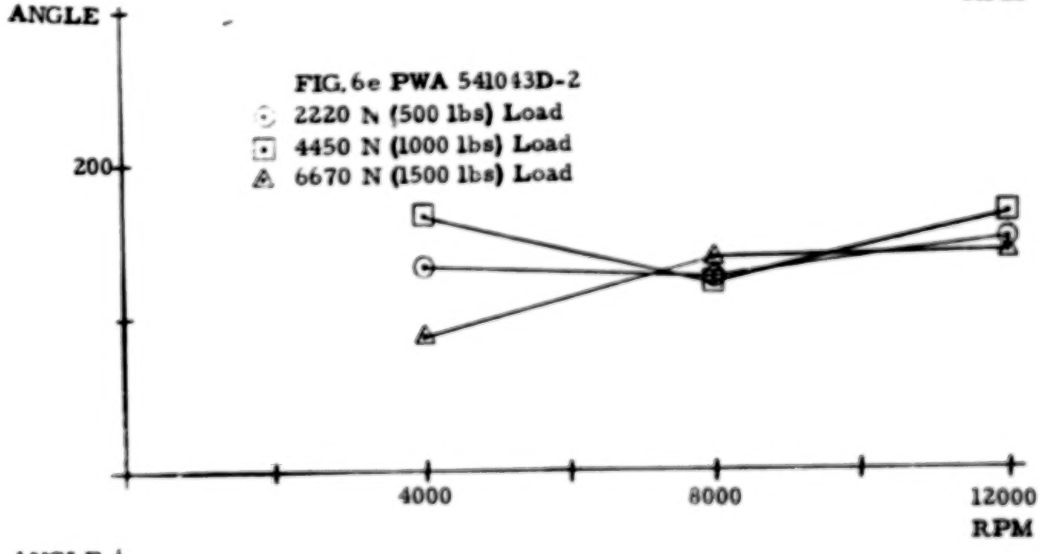

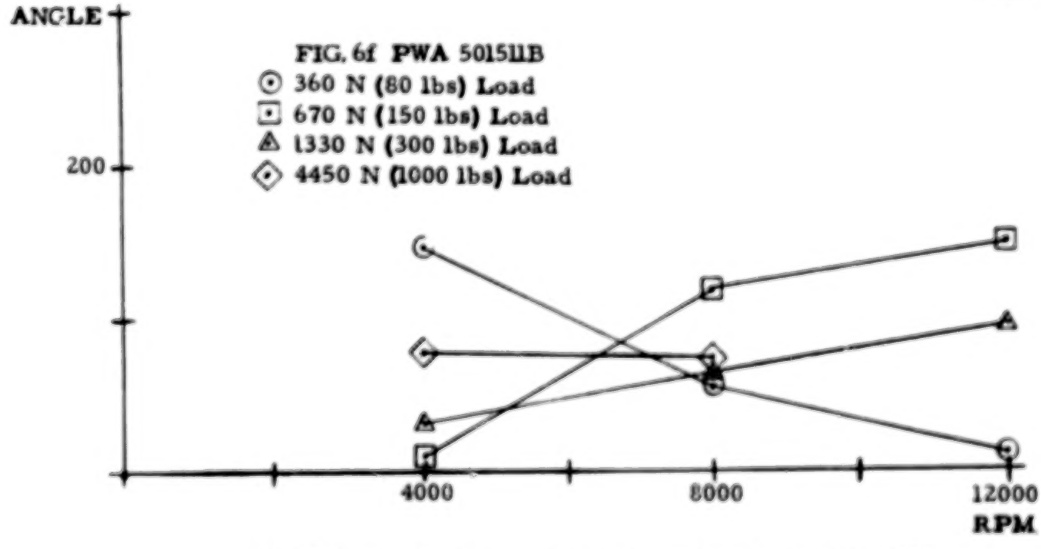

FIGS. 6d-f Resultant Cage Force Location Versus Shaft Speed

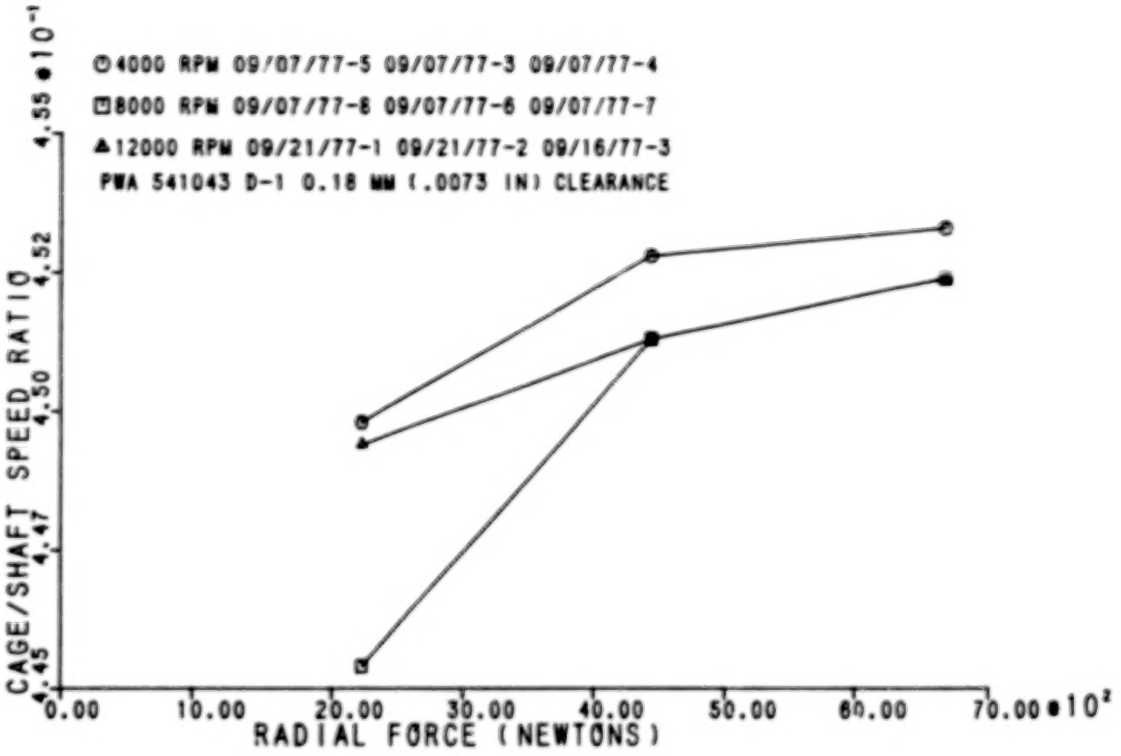

FIG. 7a Cage to Shaft Speed Ratios

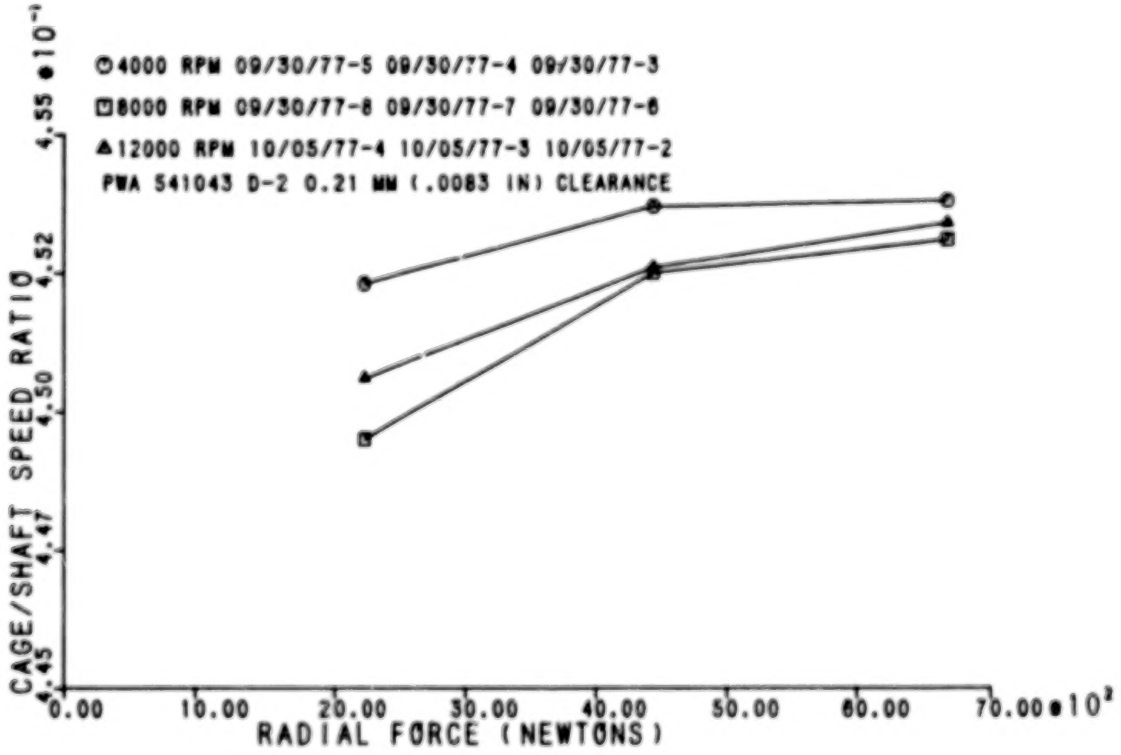

FIG. 7b Cage to Shaft Speed Ratios

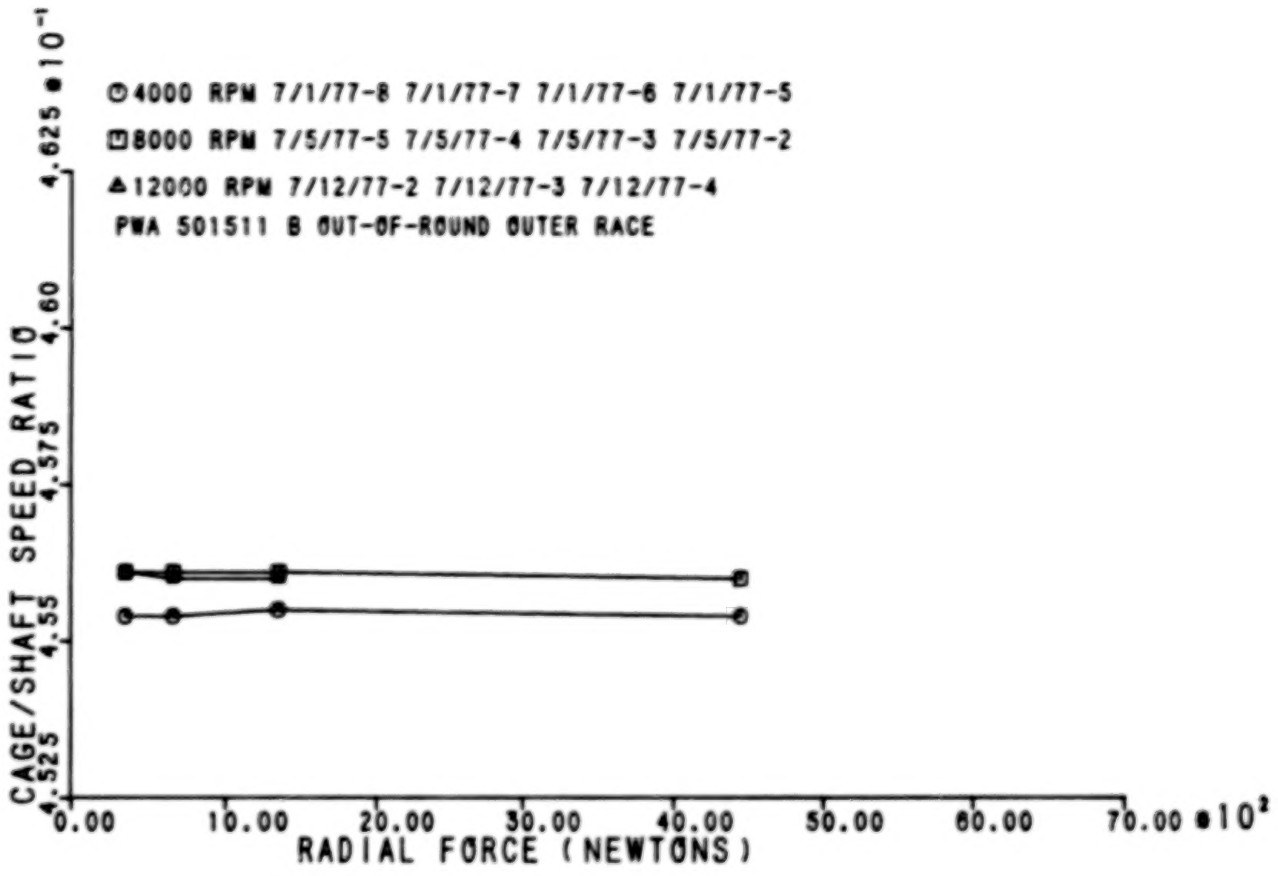

FIG. 7c Cage to Shaft Speed Ratios

Table 1
Test Bearing Specifications

	PWA 541043 D			PWA 501511 B		
	mm	inches		mm	inches	
Inner Race						
Bore Dia.	118	4.6457		115	4.5276	
Raceway Dia.	131.66	5.1834		125.79	4.9525	
Flange Dia.	137.47	5.4122		130.33	5.131	
Width	26.92	1.060		26.95	1.061	
Groove Width	14.59	.5746		11.85	.4667	
Flange Angle	0 deg.			0 deg.		
Outer Race						
Outer Dia.	164.49	6.4760		179.97	6.8884	Max**
Raceway Dia. mm (in)	157.08	6.1842	Nominal	174.90	6.8858	Min**
	157.14	6.1865	Ser. A2284*	149.67	5.8925	Max**
	157.16	6.1874	Ser. A2279*	149.96	5.9038	Min**
Width	23.9	.942		23.98	.944	
Rollers						
Diameter	12.65	.4979		11.99	.4722	
Length - overall	14.56	.5733		11.78	.4638	
- effective	13.04	.5133		10.72	.422	
- flat	8.40	.3307				
Crown Radius	622.3	24.5				
End Radius	inf.	inf.				
Number	28			28		
Cage						
Land Dia.	137.95	5.4312		131.11	5.162	
Axial Pocket Clearance	.28	.011		.46	.018	
Tangential Pocket Clearance	.221	.0087		.23	.009	
Single Rail Width	4.6	.18		5.8	.23	

*Bearing Serial Number A2284 has clearance .18 mm (.0073 in), is designated PWA 541043 D-1 in figures.
Bearing Serial Number A2279 has clearance .21 mm (.0083 in), is designated PWA 541043 D-2 in figures.
Clearance is outer race inner diameter minus 2 roller dia. minus inner race outer diameter.
**PWA 501511 B has out-of-round outer raceway.

Table 2

Summary of Test Conditions and Data

Fig.	Bean	Speed RPM	Load N	Load (lb)	Resultant Cage Force Magnitude N	Resultant Cage Force Magnitude (lb)	Resultant Cage Force Location Degrees	Cage/Shaft Speed Ratio ω_c/ω_s	Cage Slip %
					FWA 541043 D-1 0.18 mm (0.0073 in) Clearance				
3a	A	4000	2200	500	7.29	1.64	154	.4498	1.4
b	A	4000	4450	1000	2.76	.62	142	.4528	.7
c	A	4000	6670	1500	9.73	2.19	150	.4533	.6
d	A	8000	2220	500	43.38	9.76	136	.4454	2.4
e	A	8000	4450	1000	17.96	4.04	118	.4513	1.1
f	A	8000	6670	1500	24.36	5.48	91	.4524	.8
g	A	12000	2220	500	59.96	13.49	153	.4494	1.5
h	A	12000	4450	1000	60.41	13.59	164	.4513	1.1
i	A	12000	6670	1500	42.27	9.51	145	.4524	.8
j	C	4000	360	80	9.11	2.05	45	.3959	13.2
k	C	4000	670	150	4.13	.93	27	.4093	10.3
l	C	4000	1330	300	11.25	2.53	167	.4378	4.0
m	C	4000	4450	1000	9.29	2.09	148	.4527	.8
n	C	8000	360	80	21.82	4.91	33	.3802	16.5
o	B	4000	2220	500	24.85	5.59	167	.4509	1.2
p	B	4000	4450	1000	21.34	4.80	113	.4520	.9
q	B	4000	6670	1500	20.18	4.54	121	.4534	.6
r	B	8000	2220	500	104.85	23.59	156	.4478	1.8
s	B	8000	4450	1000	76.85	17.29	148	.4519	.9
t	B	8000	6670	1500	80.72	18.16	162	.4532	.7
					FWA 541043 D-2 0.21 mm (.0083 in) Clearance				
4a	A	4000	2220	500	11.73	2.64	133	.4523	.8
b	A	4000	4450	1000	8.00	1.80	166	.4537	.5
c	A	4000	6670	1500	7.69	1.73	88	.4539	.5
d	A	8000	2220	500	44.36	9.98	127	.4495	1.5
e	A	8000	4450	1000	52.05	11.71	123	.4525	.8
f	A	8000	6670	1500	35.03	7.88	139	.4531	.7
g	A	12000	2220	500	25.25	5.68	149	.4506	1.2
h	A	12000	4450	1000	52.10	11.72	167	.4526	.8
i	A	12000	6670	1500	23.83	5.36	141	.4527	.8
					FWA 501511 B Out-Of-Round Outer Raceway				
5a	C	4000	360	80	6.62	1.49	147	.4554	.2
b	C	4000	670	150	2.13	.48	11	.4554	.2
c	C	4000	1330	300	2.19	.49	32	.4555	.2
d	C	4000	4450	1000	8.31	1.87	78	.4554	.2
e	C	8000	360	80	13.20	2.97	55	.4561	.1
f	C	8000	670	150	8.40	1.89	118	.4561	.1
g	C	8000	1330	300	14.62	3.29	65	.4561	.1
h	C	8000	4450	1000	18.58	4.18	74	.4560	.1
i	C	12000	360	80	2.67	.60	11	.4561	.1
j	C	12000	670	150	2.04	.46	149	.4560	.1
k	C	12000	1330	300	11.96	2.69	95	.4560	.1

Bean A has K = 79.5 N/mm (454 lb/in)
Bean B has K = 29.3 N/mm (160 lb/in)
Bean C has K = 22.8 N/mm (130 lb/in)

Table 3

Calculated Number of Shaft Revolutions Between Photographs
For Bearings with Epicyclic Speed Ratio of 0.456

$\Delta\theta_o$ rev	$W_s=(\Delta\theta_o)\frac{16 \times 60}{.441}$	$\Delta\theta_s$ rev	$W_s=(\Delta\theta_s)\frac{16 \times 60}{(-.559)}$
0 to 1	0 to 2,234 rpm	0 to -1	0 to 1,877 rpm
1 to 2	2,234 to 4,469	-1 to -2	1,877 to 3,753
2 to 3	4,469 to 6,703	-2 to -3	3,753 to 5,630
3 to 4	6,703 to 8,938	-3 to -4	5,630 to 7,507
4 to 5	8,938 to 11,884	-5 to -6	7,507 to 9,383
5 to 6	11,173 to 13,407	-6 to -7	9,383 to 11,260
		-7 to -8	11,260 to 13,137

1. Report No.	2. Government Accession No.	3. Recipient's Catalog No.
NASA CR-3048		

4. Title and Subtitle	5. Report Date
ROLLER TO SEPARATOR CONTACT FORCES AND CAGE TO SHAFT SPEED RATIOS IN ROLLER BEARINGS	September 1978
	6. Performing Organization Code
7. Author(s)	8. Performing Organization Report No.
Leslie J. Nypan	
	10. Work Unit No.
9. Performing Organization Name and Address	11. Contract or Grant No.
California State University, Northridge Northridge, California 91330	NSG-3065
	13. Type of Report and Period Covered
12. Sponsoring Agency Name and Address	Contractor Report
National Aeronautics and Space Administration Washington, D.C. 20546	14. Sponsoring Agency Code

15. Supplementary Notes

Final report. Project Manager, Harold H. Coe, Fluid System Components Division, NASA Lewis Research Center, Cleveland, Ohio 44135.

16. Abstract

Cage to roller force measurements, cage to shaft forces, and cage to shaft speed ratios are reported for 115- and 118-mm bore roller bearings operating at speeds of 4000, 8000, and 12 000 rpm under loads ranging from 360 to 6670 N (80 to 1500 lb).

17. Key Words (Suggested by Author(s))	18. Distribution Statement
Roller bearings Cage forces Cage speed Roller-cage contact	Unclassified - unlimited STAR Category 37

19. Security Classif. (of this report)	20. Security Classif. (of this page)	21. No. of Pages	22. Price*
Unclassified	Unclassified	71	A04

* For sale by the National Technical Information Service, Springfield, Virginia 22161

NASA-Langley, 1978

END

FEB 28, 1979